Heterozygous LmnadelK32 mice develop dilated cardiomyopathy through a combined pathomechanism of haploinsufficiency and peptide toxicity.

Marie-Elodie Cattin, Anne T Bertrand, Saskia Schlossarek, Marie-Catherine Le Bihan, Søren Skov Jensen, Christiane Neuber, Claudia Crocini, Sophia Maron, Jeanne Lainé, Nathalie Mougenot, et al.

Heterozygous *Lmna*^{delK32} mice develop dilated cardiomyopathy through a combined pathomechanism of haploinsufficiency and peptide toxicity

Marie-Elodie Cattin[1,2], Anne T. Bertrand[1,2], Saskia Schlossarek[3], Marie-Catherine Le Bihan[1,2,4], Søren Skov Jensen[4], Christiane Neuber[3], Claudia Crocini[3], Sophia Maron[3], Jeanne Lainé[1,2,5], Nathalie Mougenot[6], Shaïda Varnous[1,2], Yves Fromes[1,2], Arne Hansen[3], Thomas Eschenhagen[3], Valérie Decostre[1,2], Lucie Carrier[1,2,3,†] Gisèle Bonne[1,2,7, †,*.]

[1]Inserm, U974, Paris F-75013, France. [2]Université Pierre et Marie Curie- Paris 6, UM 76, CNRS, UMR 7215, Institut de Myologie, IFR14, Paris F-75013, France. [3]Department of Experimental Pharmacology and Toxicology, Cardiovascular Research Center, University Medical Center Hamburg-Eppendorf, Hamburg D-20246, and DZHK (German Centre for Cardiovascular Research), partner site Hamburg/Kiel/Lübeck, Germany. [4]Department of Biochemistry and Molecular Biology, University of Southern Denmark, Odense DK-5230, Denmark. [5]UPMC Univ Paris 06, Site Pitié-Salpêtrière, Département de Physiologie, Paris F-75013 France. [6]PECMV, Inserm, IFR14, Paris F-75013, France. [7]AP-HP, Groupe Hospitalier Pitié-Salpêtrière, U.F. Cardiogénétique et Myogénétique, Service de Biochimie Métabolique, Paris F-75013, France.

[†] *These authors contributed equally to the work*

[*]To whom correspondence should be addressed:

Gisèle Bonne

Thérapie des maladies du muscle strié,

Inserm, U974, Institut de Myologie, G.H. Pitié-Salpêtrière,

47 boulevard de l'Hôpital,

F-75 651 Paris Cedex 13, France.

Tel: (33) 142165723; Fax: (33) 142165700; Email: g.bonne@institut-myologie.org.

Figure 1.

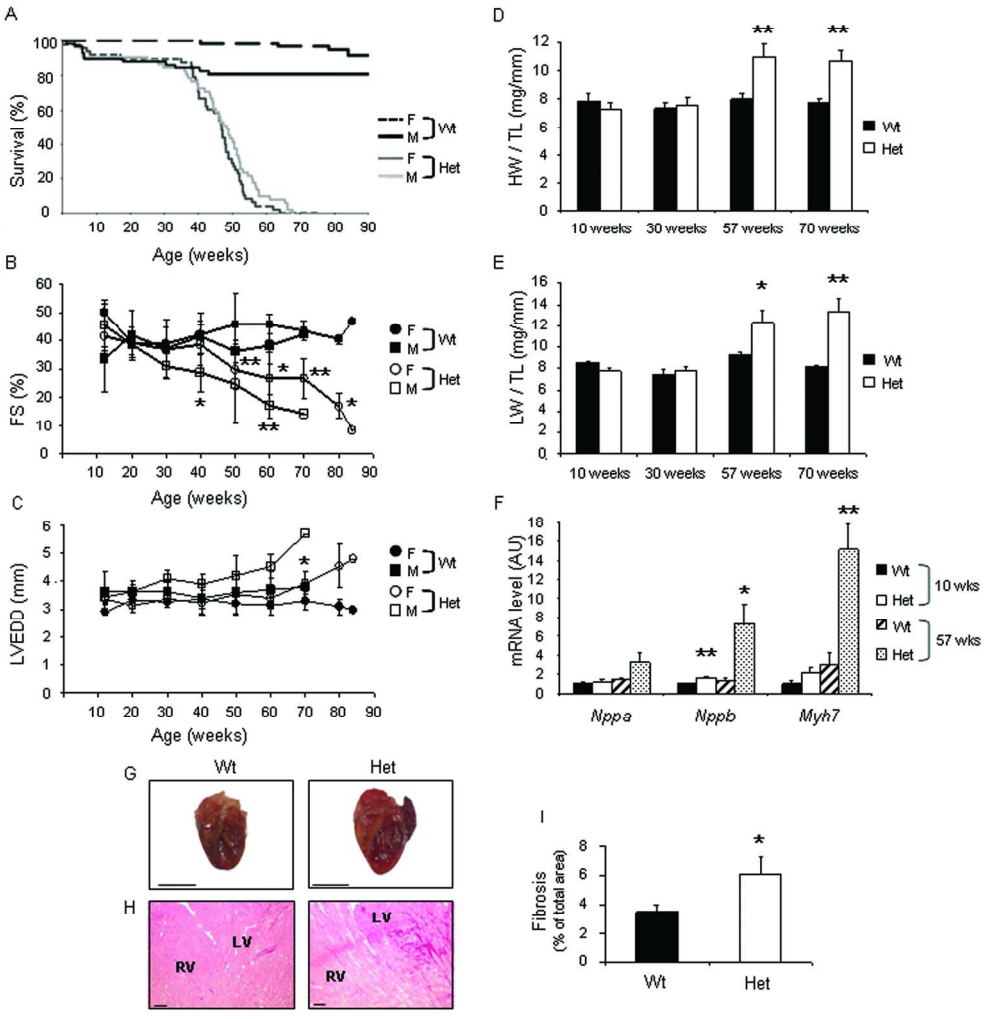

Figure 1. Cardiac phenotype of Het mice.

(A) Survival curve of Wt (57 males, 58 females) and Het (51 males, 48 females) mice. (B-C) Serial echocardiography from 12 weeks of age until death in males and females Wt (n=6 per gender) and Het (n=9 per gender) mice. (B) Fractional shortening. (C) Left ventricular end-diastolic diameter. *p<0.05, **p<0.01 compared with age- and gender-matched Wt. Mean±SD. (D) Heart weight (HW) to tibia length (TL) ratio in Wt and Het mice. (E) Lung weight (LW) to TL ratio in Wt and Het mice (n=6-17 per group) *p<0.05 **p<0.01 compared with age-matched Wt. Mean±SEM. (F) Expression of cardiac remodelling mRNA markers *Nppa, Nppb* and *Myh7* in 10 and 57 week-old Wt and Het mice (n=5-6 per group). *p<0.05, **p<0.01 compared with age-matched Wt. Mean±SEM. (G) Coronal section of Wt and Het hearts at 57 weeks of age (bar = 5 mm). (H) Cross-section of Wt and Het hearts at 57 weeks of age stained with Sirius Red (RV = right ventricle, LV = left ventricle, bar = 100 μm). (I) Proportion of fibrosis normalized to total cardiac area of 57 week-old mice (n=6 per group). *p<0.05 compared with Wt. Mean±SD.

180x193mm (300 x 300 DPI)

Figure 2.

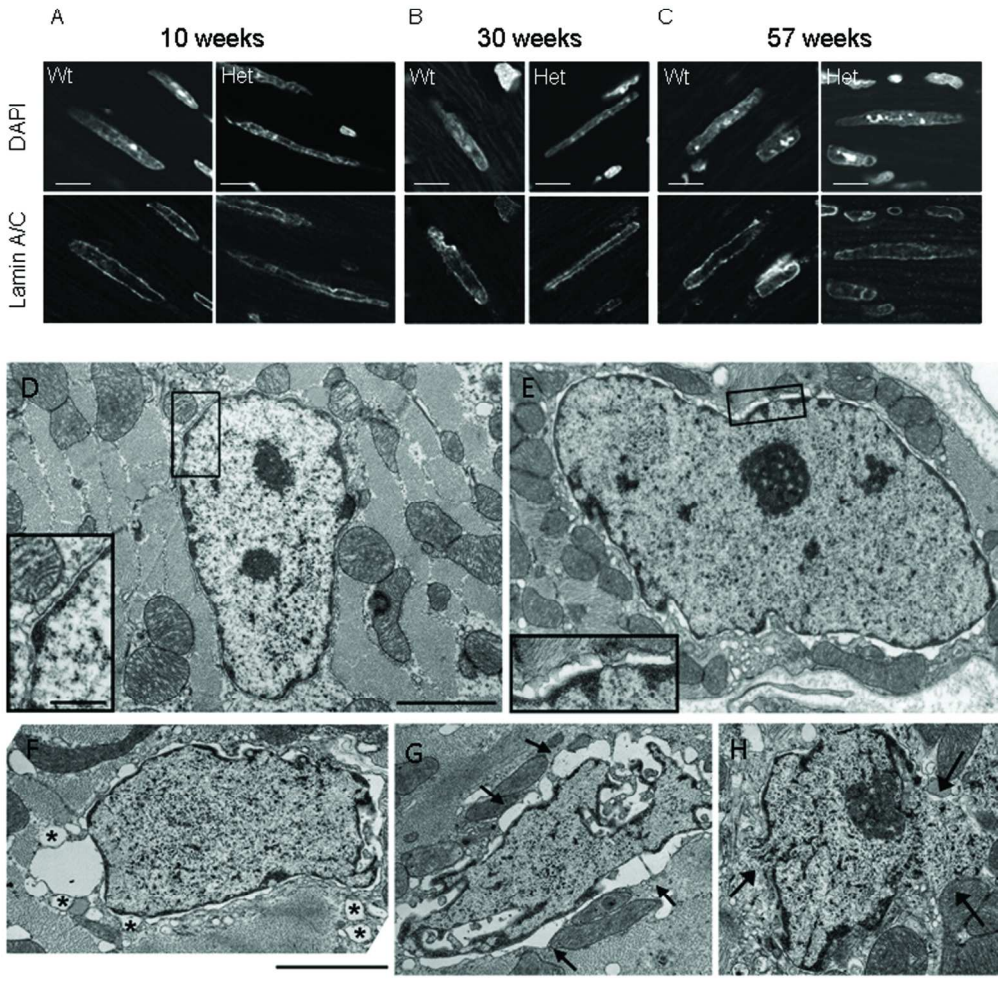

Figure 2. Lamin A/C localization and nuclear morphology in Wt and Het hearts.
(A-C) Lamin A/C staining in Wt and Het hearts before (10 weeks, A), at early-stage (30 weeks, B) and at end-stage of DCM (57 weeks, C). Nuclei are counterstained with DAPI (bar = 10µm).
(D-H) Ultrastructural features of myocardial nuclei of 12 week-old Wt (D) and Het (E) mice and 26 week-old Het mice (F-H). Widened nuclear intermembrane space (inset 2E compared with 2D, and G, arrows), large vacuoles surrounding the nucleus (F, asterisks), nuclear membrane rupture and chromatin exit (H, arrows) (bar = 2 µm and 500 nm in insets).

180x193mm (300 x 300 DPI)

Figure 3.

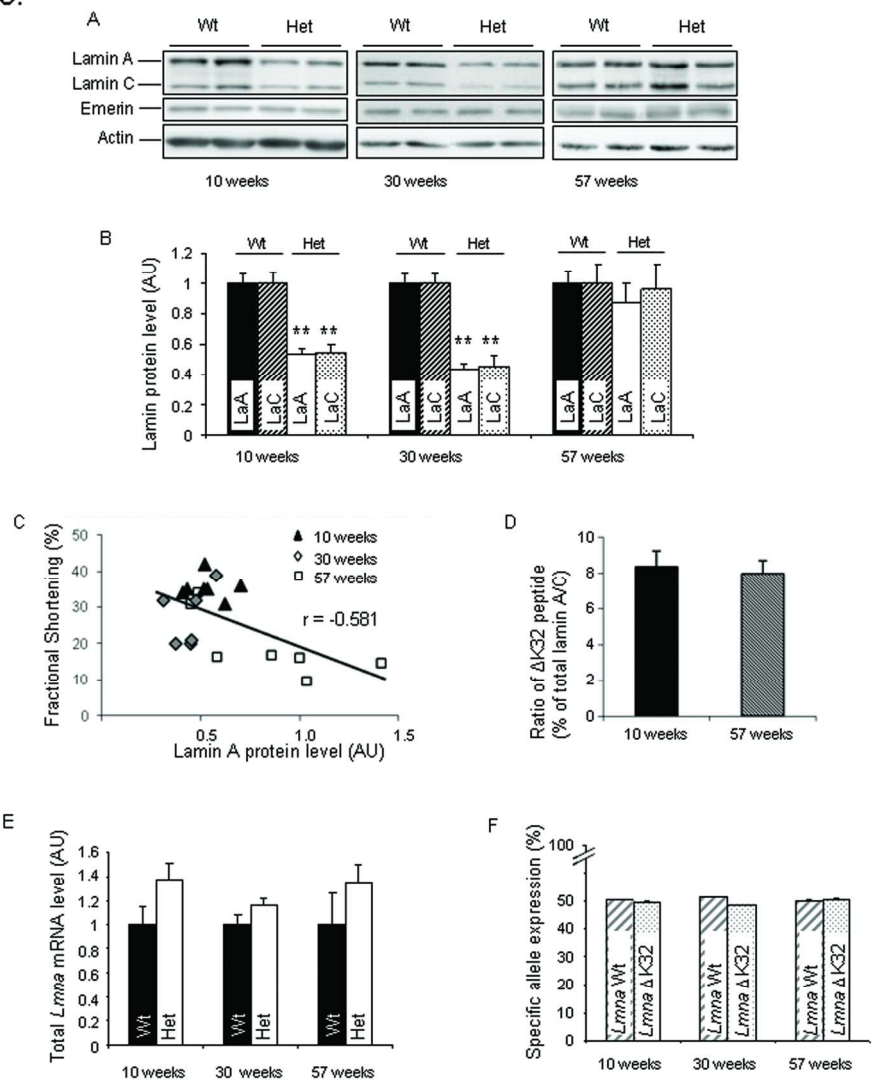

Figure 3. Evolution of mutant lamin A/C expression.

(A-B) Lamin A and C, emerin protein levels in the heart of 10, 30 and 57 week-old Het and Wt mice. Actin is used as loading control. Representative blots (A) and quantification (B) of total lamin A (LaA) and C (LaC). (n=6-9 per group). ** $p<0.01$ compared with Wt. Mean±SEM. (C) Correlation between the lamin A protein level and fractional shortening in Het mice at the 3 ages. (D) Ratio of mutant ΔK32-lamin A/C to total lamin A/C quantified by mass spectrometry based label-free quantification in the heart of 10 and 57 week-old Het mice (n=7-9 per group). Mean±SEM. (E) Level of total *Lmna* mRNA in the heart of 10, 30 and 57 week-old Het and Wt mice (n=5-6 per group). Mean±SEM. (F) Ratio of specific allele level in the heart of 10, 30 and 57 week-old Het mice. Wt allele = *Lmna* Wt, mutant allele = *Lmna* ΔK32.

180x201mm (300 x 300 DPI)

Figure 4.

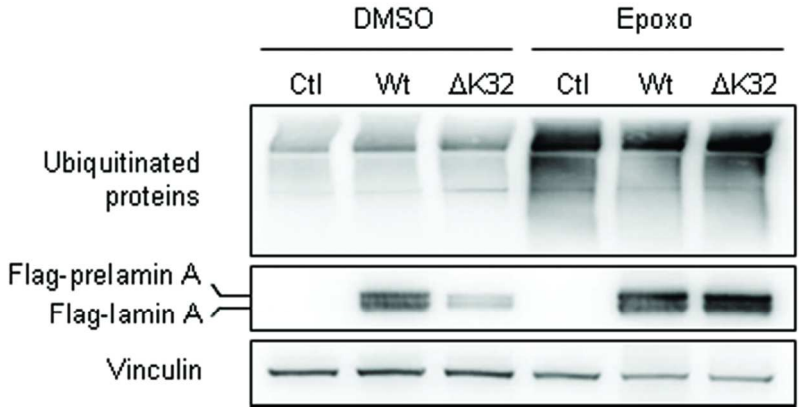

Figure 4. Effect of UPS inhibition on ΔK32-lamin A/C expression in neonatal mouse cardiomyocytes.

Ubiquitinated proteins, Flag-prelamin A and Flag-lamin A protein levels in untransduced (Ctl), Flag-Wt- (Wt) or Flag-ΔK32-lamin A (ΔK32) transduced NMCM treated with epoxomicin (epoxo) or DMSO as vehicle control. Vinculin was used as loading control.

99x47mm (300 x 300 DPI)

Figure 5.

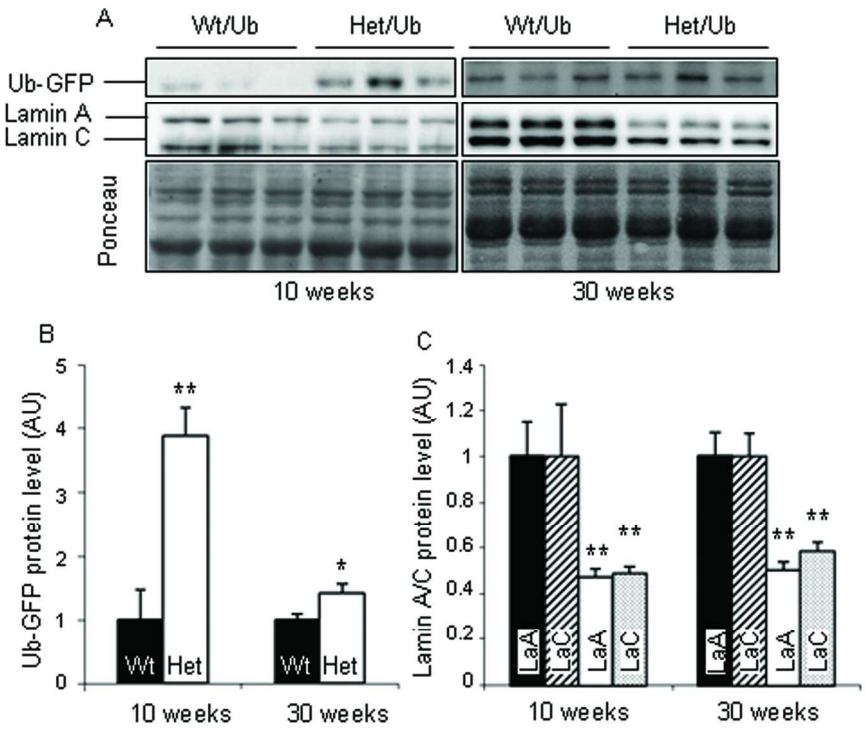

Figure 5. Global impairment of UPS in the heart of Het/Ub-GFP crossed mice.
(A) Western blots showing Ub-GFP, lamin A/C and Ponceau staining from heart of 10 and 30 week-old Wt/Ub-GFP and Het/Ub-GFP mice. (B-C) Quantification of Ub-GFP protein level (B), lamin A (LaA) and C (LaC) protein level (C). *p<0.05, ** p<0.01 Mean±SEM. Value are normalized to age-matched Wt/Ub-GFP (n=8-3 per group).

180x152mm (300 x 300 DPI)

Figure 6.

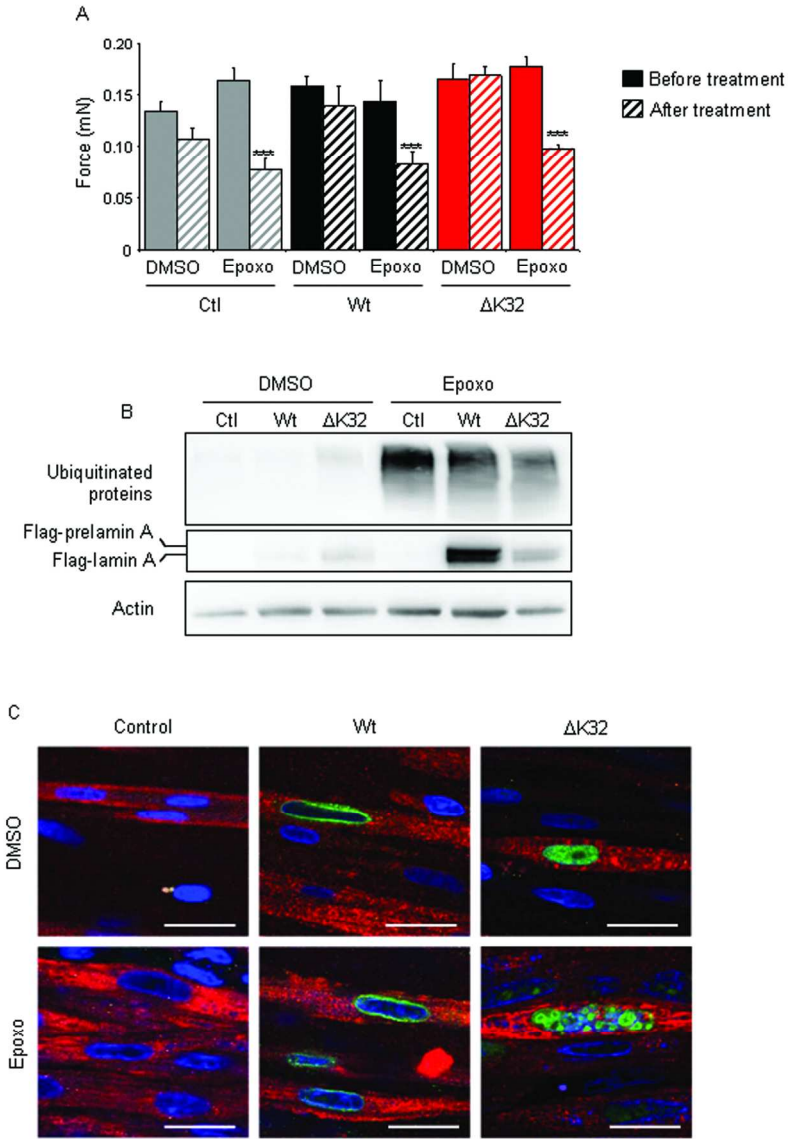

Figure 6. Effect of UPS inhibition and mutant lamin A/C overexpression on rat engineered heart tissue.

(A) Force of contraction of untransduced (Control; grey bars), Flag-Wt-lamin A (Wt; black bars) or Flag-ΔK32-lamin A (ΔK32; red bars) transduced EHTs after treatment with epoxomicin (epoxo; hatched bars) or DMSO (solid bars) as vehicle . ***p<0.001 between before and after DMSO or epoxo treatment. Mean±SEM (n=5-6 per group). (B) Representative western blot showing ubiquitinated proteins, Flag-prelamin A and Flag-lamin A protein levels in control, Wt and ΔK32 EHTs, treated with epoxomicin (epoxo) or DMSO as vehicle. Actin is used as loading control. (C) Immunostaining with anti-myosin heavy chain (red) and anti-Flag (green) antibodies. Nuclei are counterstained with DAPI (bar = 20μm).

180x220mm (300 x 300 DPI)

Figure 7.

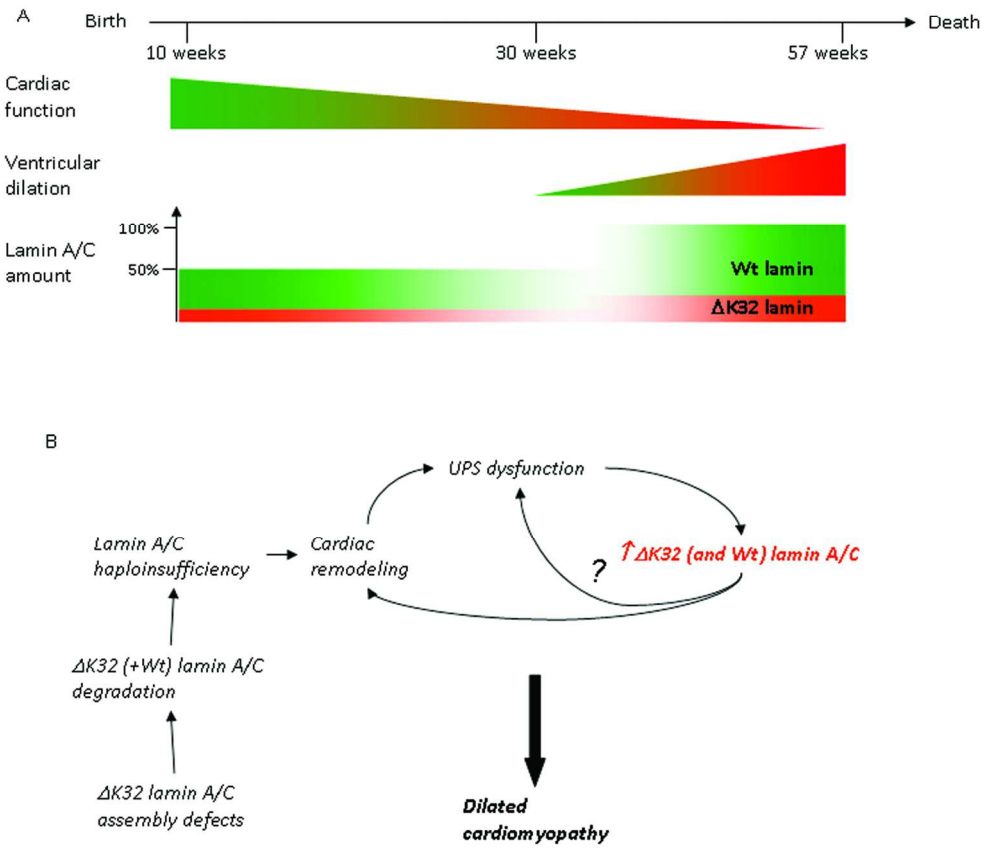

Figure 7. Schematic model of pathophysiological mechanisms linking ΔK32 lamin A/C to DCM. (A) Chronology of pathological events occurring in the heart of Het mice. (B) Working model suggesting that ΔK32 lamin A/C might disturb the assembly into protofilaments and thus be targeted for degradation (alone and/or associated to Wt lamin). It results in haploinsufficiency likely contributing to myocardial vulnerability, promoting remodelling mechanisms. These processes might have global deleterious effects, as UPS impairment. Wt and ΔK32-lamin A/C amount then increases, playing additional negative effects on cardiomyocytes function. This might precipitate cardiac dysfunction and UPS dysfunction (?), leading to DCM.

180x168mm (300 x 300 DPI)

ABSTRACT

Dilated cardiomyopathy (DCM) associates left ventricular dilatation and systolic dysfunction and is a major cause of heart failure and cardiac transplantation. *LMNA* gene encodes lamins A/C, proteins of the nuclear envelope. *LMNA* mutations cause DCM with conduction and/or rhythm defects. The pathomechanisms linking mutations to DCM remain to be elucidated. We investigated the phenotype and associated pathomechanisms of heterozygous $Lmna^{\Delta K32/+}$ (Het) knock-in mice, which carry a human mutation. Het mice developed a cardiac-specific phenotype. Two phases, with two different pathomechanisms, could be observed that lead to the development of cardiac dysfunction, DCM and death between 35 and 70 weeks of age. In young Het hearts, there was a clear reduction in lamin A/C level, mainly due to the degradation of toxic ΔK32-lamin. As a side effect, lamin A/C haploinsufficiency probably triggers the cardiac remodelling. In older hearts, when DCM has developed, lamin A/C level was normalized and associated with increased toxic ΔK32-lamin expression. Crossing our mice with the Ub^{G76V}-GFP UPS reporter mice revealed a heart-specific UPS impairment in Het. While UPS impairment itself has clear deleterious effect on engineered heart tissue's force of contraction, it also leads to the nuclear aggregation of viral-mediated expression of ΔK32-lamin. In conclusion, Het mice are the first knock-in *Lmna* model with cardiac-specific phenotype at the heterozygous state. Altogether, our data provide evidence that Het cardiomyocytes have to deal with major dilemma: mutant lamin A/C degradation or normalization of lamin level to fight the deleterious effect of lamin haploinsufficiency, both leading to DCM.

INTRODUCTION

The main features of dilated cardiomyopathy (DCM) are left ventricular dilatation, systolic dysfunction, myocyte death and myocardial fibrosis. DCM represents a major cause of heart failure and cardiac transplantation. Analysis of relatives of affected patients reveals a familial disease in 20% to 35% of cases (1). Among all the mutated genes reported in familial DCM, *LMNA* gene represents one of the first known cause of non-syndromic DCM in patients, estimated at 6% of DCM (1). The *LMNA*-related cardiomyopathy associates DCM, conduction and/or rhythm defects (DCM-CD) (2, 3) and is mainly dominantly inherited.

To date, more than 450 *LMNA* gene mutations have been reported (http://www.umd.be/LMNA/), which lead to a wide spectrum of diseases collectively referred to as laminopathies (4). These pathologies involve either specific tissues (striated muscles, adipose tissue, peripheral nerves) or several systems (progeroid syndromes) with overlapping phenotypes. Among the *LMNA* mutations identified so far, most of them lead to cardiac diseases (DCM-CD) isolated or associated with skeletal muscles involvement, e.g. *LMNA*-related congenital muscular dystrophy (5), Emery-Dreifuss muscular dystrophy (EDMD) (6) and limb-girdle muscular dystrophy (7). In those pathologies, DCM-CD constitutes the most serious and life-threatening manifestation of the disease.

LMNA encodes A-type lamins, mainly comprising lamins A and C (8). Lamins A/C are ubiquitous proteins of the type V intermediate filament family. They assemble in highly organized structures and, together with B-type lamins, form a meshwork beneath the inner nuclear membrane: the nuclear lamina (9). The physiological roles of lamin A/C are not yet fully understood. Their numerous interactions with proteins of the nuclear membrane support a role in maintaining the structure and stiffness of the nuclear envelope. They also largely interact with proteins of the nucleoplasm (transcription factors and histones) and with chromatin, which suggests physiological functions in regulation of gene expression (9, 10).

The mechanisms by which mutations in *LMNA* lead to tissue-specific diseases remain unclear. An important function of the nuclear lamina is to maintain the structural integrity of cells. Therefore, lamina defects might result in cellular “weakness” and damages, critical for muscular cells subjected

to constant mechanical stress. In addition, altered tissue-specific gene expression might also be involved in the diseases (9). Cumulative evidence indicates that the steady-state level of lamin A/C is crucial for normal cell morphology and function, especially in the heart. Overexpression of wild-type lamin A/C in cells and tissues leads to nuclear abnormalities and higher sensitivity to cell death (11, 12). *Lmna*$^{-/-}$ mice develop severe DCM and die prematurely at 8 weeks of age (13), and heterozygous *Lmna*$^{+/-}$ mice that express only 50% of lamin A/C suffer from DCM-CD arising at adulthood (14, 15).

We created a new *Lmna* mutant mouse model deleted for lysine 32 of lamin A/C (*Lmna*$^{\Delta K32}$ mouse) (16). Homozygous *Lmna*$^{\Delta K32/\Delta K32}$ mice exhibit maturation defects of skeletal and cardiac muscles, and severe metabolic disorders responsible for premature death at 2 weeks of age, suggesting that the ΔK32-lamin A/C protein itself and/or the overall reduction in lamin A/C level (-80%) has deleterious effects (16). At this age, heterozygous *Lmna*$^{\Delta K32/+}$ mice did not have an obvious pathological phenotype. In the present paper, we further investigated the phenotype of the heterozygous *Lmna*$^{\Delta K32/+}$ adult mice (thereafter called Het mice).

RESULTS

Absence of skeletal muscle or metabolic defects in Het mice

As *Lmna*$^{\Delta K32/\Delta K32}$ mice showed skeletal muscle abnormalities (16), we investigated the skeletal muscle phenotype of old Het mice (57 weeks of age). Spontaneous activity test, *in vitro* contractile function of diaphragm, *soleus* and *extensor digitorum longus* muscles, and histological analysis of *gastrocnemius* muscle were performed in Het and Wt mice (Supplemental table 1 and supplemental Fig 1). All these parameters did not differ between Het and Wt mice, suggesting no skeletal muscle defect in Het mice. However, the lamin A/C protein level in *gastrocnemius* was more than 50% lower in Het than in Wt mice (Supplemental Fig 2). In addition, Het mice showed no evidence of organ abnormalities (normal weight and aspect of liver, kidney, spleen, skin and vasculature) or metabolic disorders (normal fat deposition and glycaemia, triglycerides and cholesterol levels in serum; data not shown).

Development of dilated cardiomyopathy in Het mice

Het mice displayed a shortened lifespan, dying between 35 and 70 weeks of age without gender-difference (Fig 1A). To assess the cardiac phenotype, we performed echocardiographic and electrocardiographic (ECG) longitudinal studies of male and female Het and Wt mice from 12 weeks of age until death. These revealed a progressive development of cardiac dysfunction in Het mice, as shown by decreased fractional shortening (FS), which started a bit earlier in males than in females (Fig 1B; Supplemental Tables 1 and 2). This was followed by increased left ventricular end-diastolic diameter (LVEDD; Fig 1C; Supplemental Tables 2 and 3). These features matched with a DCM phenotype. Despite left ventricular (LV) dilation, there was no major wall thinning (IVSd and PWd; Supplemental Tables 2 and 3). Importantly, whatever the age of onset of cardiac dysfunction (from 32 to 70 weeks of age), the timeline of the disease evolution was very reproducible between mice, i.e. 15-20 weeks between reduced FS and death. Surface ECG recordings did not reveal any conduction or rhythm defect in Het mice. Some unspecific abnormalities (slight bradycardia, higher PR interval, QRS complex broadening) were observed at the very end-stages of the DCM only (data not shown).

The progression of DCM was associated with cardiac hypertrophy (Fig 1D) and ventricular and atrial enlargement (Fig 1G) in both males and females. At the end stage, the LV of Het mice presented slight fibrosis (Fig 1H and 1I). Het mice eventually presented with congestive heart failure as demonstrated by marked LV hypokinesia and lung oedema reflected by increase in lung weight to tibia length ratio (Fig 1E). Analysis of mRNA levels of cardiac remodelling markers at 10 and 57 weeks revealed no change in *Nppa* mRNA level, whereas *Nppb* mRNA amounts were higher in Het than in Wt mice at both ages (Fig 1F). *Myh7* mRNA level did not differ between 10 week-old Het and Wt, but was 5-fold higher in 57 week-old Het mice. These results suggest that cardiac remodelling has already started at 10 weeks of age in Het mice.

Abnormal nuclear shape in Het hearts

Immunostaining analysis of lamin A/C in the heart of 10, 30 and 57 week-old Het mice revealed nuclear rim localization similar to age-matched Wt (Fig 2). However, a large proportion of nuclei were more elongated and thinner in Het than in Wt hearts at all ages (Fig 2), even before the onset of DCM (Fig 2A). Myocardial ultrastructure analysed by electron microscopy revealed preserved sarcomeric architecture, but many elongated nuclei with enlarged nuclear intermembrane space in young asymptomatic Het mice compared with Wt (Fig 2D and E). In Het animals with mild cardiac dysfunction, severe alterations were found in many nuclei, such as extremely enlarged nuclear intermembrane space, accumulation of large perinuclear vacuoles (Fig 2F and G), or envelope rupture with extravasations of chromatin into the cytoplasm (Fig 2H). At the end-stage, in addition to the pronounced alteration of a majority of nuclei, nonspecific degenerative changes were observed: disrupted sarcomeres, myofibrillar lysis, vesicular proliferation of sarcomeric reticulum, intracytoplasmic junctions, electron dense residual bodies and pericellular fibrosis (data not shown).

Modulation of lamin A/C level with the progression of dilated cardiomyopathy

We evaluated the amount of lamin A/C proteins in the heart of 10, 30 and 57 week-old Het and Wt mice. Cardiac lamin A/C level did not change with aging in Wt mice (data not shown). In contrast,

whereas cardiac lamin A/C level was 50% lower in 10 and 30 week-old Het than in age-matched Wt mice, it did not differ between 57-week-old Het and Wt mouse hearts (Fig 3A and B). Furthermore, the level of lamin A was negatively correlated with the fractional shortening in Het hearts (Fig 3C; r=-0.581; Pearson correlation test $p<0.01$). These data suggest that progression of DCM is associated with an increase in the total (wild-type and mutant) lamin A/C level in Het hearts. This normalization of lamin A/C level was not due to an increase in the number of cells in Het hearts, as the level of emerin, another nuclear protein, did not differ in Het and Wt hearts at all tested ages (Fig 3A). In order to determine the relative amount of ΔK32-lamin A/C in the heart, mass spectrometry (MS) was employed (Fig 3D and Supplemental Fig 3-4). Lamin A/C peptides were generated by trypsin digestion of protein extracts from heart samples of Het mice. Analysis of peptide signal intensities from the two unique Wt-peptides (^{33}EDLQELNDR^{41} and ^{29}LQE**K**EDLQELNDR^{41}) and from the unique ΔK32-peptide (^{29}LQEEDLQELNDR^{40}) showed that the ΔK32-peptide represented 8.4% and 8% of total lamin A/C proteins in the heart of 10 and 57 week-old Het mice, respectively (Fig 3D). This indicates that the ratio of ΔK32-to-total lamin A/C was very low in Het hearts throughout the evaluated lifespan. Furthermore, the MS quantification confirmed that the overall amount of total lamin A/C increased (1.5-fold change) with age in Het mice (Supplemental Fig 4E), as observed by western blot (Fig 3A and B). This suggests that the absolute amount of ΔK32-lamin A/C increased in 57 compared to 10 week-old Het hearts.

We then evaluated whether modulation of total lamin A/C protein and reduced ΔK32-lamin A/C expression were due to modulation of *Lmna* gene expression. Total *Lmna* mRNA level did not differ between Het and Wt mice at 10, 30 and 57 weeks of age (Fig 3E). Of note, *Lmna* mRNA was equally expressed in Wt hearts at all tested ages. Allele-specific mRNA level assessment by RT-qPCR showed that both alleles were equally expressed in the heart of Het mice at the three stages (Fig 3F). This suggests that the lower lamin A/C protein level in young Het hearts results from post-transcriptional regulations. We thus hypothesized that i) in young Het hearts, lamin A/C haploinsufficiency results from specific degradation of ΔK32-lamin A/C and ii) in old Het hearts,

normalization of lamin A/C via the increase in ΔK32-lamin A/C results from an impairment/saturation of this degradation system.

Degradation of lamin A via the ubiquitin-proteasome system in cardiomyocytes

In mammalian cells, the ubiquitin-proteasome system (UPS) is the major non-lysosomal degradation system involved in protein homeostasis (17). To determine whether the UPS was involved in the degradation of Wt or ΔK32-lamin A/C, neonatal mouse cardiomyocytes (NMCM) were transduced with adeno-associated virus serotype 6 (AAV6) encoding Flag-Wt- or Flag-ΔK32-prelamin A. The level of Flag-ΔK32-lamin A was lower than the level of Flag-Wt-lamin A (Fig 4), suggesting lower protein stability of Flag-ΔK32-lamin A. Transduced NMCM were then treated for 24 h with 500 nM of the UPS inhibitor epoxomicin. Epoxomicin treatment induced accumulation of both Flag-Wt- and Flag-ΔK32-lamin A, indicating that UPS degrades both Wt and ΔK32-lamin A in cardiomyocytes.

Impairment of the ubiquitin-proteasome system in Het hearts

We then hypothesized that the age-dependent increase in cardiac lamin A/C level is the result of heart specific UPS impairment in Het mice. To assess the global function of the UPS, Het and Wt mice were crossed with Ub^{G76V}-GFP mice. Ub^{G76V}-GFP (thereafter called Ub-GFP) mice ubiquitously express a green fluorescent protein (GFP)-based proteasome substrate that allows monitoring of the UPS *in vivo*, the Ub-GFP protein level being inversely correlated with UPS function (18). Ub-GFP level was very low in young Wt/Ub hearts and increased with age (Fig 5A), indicating a general dysfunction of the UPS with ageing. Interestingly, the Ub-GFP level was highly increased in 10 week-old Het/Ub-GFP hearts and persists thereafter although the difference was milder (Fig 5A and B). UPS impairment appeared prior to normalization of lamin A/C level in Het/Ub-GFP mice, as lamin A/C level was 50% lower than in Wt/Ub-GFP mice at these ages (Fig 5A and C). Of note, the UPS function was preserved in skeletal muscle (*gastrocnemius*) as reflected by similar Ub-GFP level in 30 week-old Het/Ub-GFP and Wt/Ub-GFP mice (Supplemental Fig 5) as well as in liver and kidney from both Het/Ub-GFP and

Wt/Ub-GFP mice (data not shown). Altogether, these results indicate that UPS impairment starts early and is strictly restricted to the heart in Het mice.

Importance of a functional UPS for EHT's contractility and for ΔK32-lamin aggregates clearance

We then hypothesized that the early UPS dysfunction is responsible for the first signs of cardiac dysfunction in young Het mice, which is worsened in old heart by the increase in ΔK32-lamin A/C. To test this hypothesis, we evaluated the contractile properties of engineered heart tissues (EHT; (19)) treated or not with an UPS inhibitor. Epoxomicin treatment (24 h) reduced force of contraction when compared to untreated EHTs (Fig 6A, grey bars), suggesting that an active UPS is required for efficient contractile function of cardiomyocytes.

We then evaluated the impact of AAV6-mediated gene transfer of Flag-Wt- and Flag-ΔK32-prelamin A on contractile properties of EHTs in the absence or presence of proteasome inhibitor. When the UPS is functional (DMSO treated EHTs), overexpression of Flag-Wt- or Flag-ΔK32-lamin did not change the force of contraction of EHTs when compared with untransduced cardiomyocytes (Fig 6A). Epoxomicin treatment leads to the increase in Flag-Wt- and Flag-ΔK32-lamin expression (Fig 6B), demonstrating that UPS is involved in the regulation of Flag-lamin A expression level in EHTs. Despite the increase in Flag-ΔK32-lamin level after epoxomicin treatment, EHTs' force of contraction did not differ from Flag-Wt-lamin and untransduced controls EHTs treated with epoxomicin (Fig 6A). This result indicates that short time increased ΔK32-lamin expression is not sufficient to worsen contractile dysfunction due to UPS inhibition in EHTs.

Immunostaining revealed a normal nuclear rim localisation of Flag-Wt-lamin in both DMSO and epoxomicin treated EHTs (Fig 6C). However, Flag-ΔK32-lamin A was located in the nucleoplasm in DMSO treated EHTs, as previously reported (16), and aggregated into large nucleoplasmic foci after UPS inhibition (Fig 6C).

These results suggest that degradation of ΔK32-lamin A via the UPS in reconstituted heart tissue limits its aggregation and its putative negative effect on contractility.

DISCUSSION

We report here that a heterozygous in-frame amino acid deletion in the N-terminal domain of lamin A/C caused a cardiac-specific phenotype in mice. We show that (i) Het mice developed a progressive cardiac dysfunction and DCM evolving to death between 35 and 70 weeks of age; (ii) young Het hearts, which are still unaffected, exhibited lamin A/C haploinsufficiency, whereas old affected Het hearts had increased lamin A/C amount; (iii) lamin A/C haploinsufficiency is in part due to ΔK32-lamin A/C (alone and/or associated with Wt A-type lamin) degradation through the UPS; (iv) Het hearts exhibited UPS impairment before DCM development; (v) UPS inhibition had deleterious effect on contractile properties of EHTs; (vi) alteration of ΔK32-lamin degradation induced its nuclear aggregation in EHTs with inhibited UPS. These data provide evidence for a major role of the UPS in the regulation of cardiac function and of lamin A/C level in the heart of Het mice that appears to be a key pathophysiological component leading to DCM in Het mice

Haploinsufficiency of lamin A/C in Het mice

Young Het mice presented with 50% less lamin A/C than age-matched Wt in heart and muscles (Fig 3, Supplemental Fig 2; (16)). With age, they developed cardiac disease but no skeletal muscles defects. This segmental phenotype affecting only cardiac muscle has already been observed in striated muscle-specific laminopathies (20). The heart seems to be more vulnerable than skeletal muscles to haploinsufficiency in patients. Indeed, genotype/phenotype correlations using *LMNA* Universal mutation database (http://www.umd.be/LMNA/) showed that 67% of nonsense and truncating mutations, which putatively lead to lower lamin A/C levels, cause cardiac diseases without muscle involvement (21-23). To date, no clear evidence explains the contrasting sensitivity to lamin A/C haploinsufficiency between the heart and skeletal muscles. It might result from structural and functional differences of these two tissues. The heart contracts in a ‘twist’ way, generating torsion whereas skeletal muscles generate unidirectional shortening. In addition, distinct organizations of the cellular cytoarchitecture and nuclei positioning (central in cardiomyocytes *vs* subsarcolemmal in muscle) result in singular forces applied on cardiac nuclei compared to myofibers. This may explain,

in part, the higher susceptibility of cardiac muscle to nuclear mechanical defects and deformations induced by loss of lamin A/C function, as observed in Het mice.

Like in human, lamin A/C haploinsufficiency induces heart disease in mouse. *Lmna*$^{+/-}$ mice, presenting 50% of lamin A/C in tissues, exhibit apoptosis of atrio-ventricular nodal myocytes and progressive electrophysiologic disease starting at 10 weeks of age (14). They also develop mild dilated cardiomyopathy (15). Like in *Lmna*$^{+/-}$ mice, part of the cardiac phenotype of Het mice can be attributed to haploinsufficiency. Jahn and colleagues (24) have recently reported that, in addition to haploinsuffisiency, *Lmna*$^{-/-}$ mice exhibited a truncated lamin A (lamin AΔ8-11) probably resulting in moderate toxic effect. Interestingly, our data show that Het mice developed a more severe phenotype than *Lmna*$^{+/-}$ mice and with several different features. Both mouse strains displayed DCM, with a relatively earlier onset for *Lmna*$^{+/-}$ mice (15). However, only 20% of *Lmna*$^{+/-}$ mice suffered from life-threatening cardiac dysfunction, whereas all Het mice died from congestive heart failure. No cardiac electrical abnormalities were observed in Het mice using surface ECG whereas *Lmna*$^{+/-}$ mice showed rhythm and conduction defects, suggesting specific mechanisms related to the deletion of lysine 32. These results suggest a stronger 'toxic' effect of ΔK32-lamin A/C compared to lamin AΔ8-11. The presence of ΔK32-lamin and its relative increase with time might lead via a toxic peptide effect to the aggravation of defects due to lamin haploinsufficiency in Het hearts.

UPS dysfunction in the heart of Het mice

Whatever the primary cause (mechanical overload, ischemia or mutant proteins), myocardial remodelling is a common feature of chronic heart failure and involves several pathways. Cumulative evidences suggest that alteration of proteasomal-mediated protein degradation contributes to the initiation and/or progression of cardiac diseases in humans and in experimental models (25). Especially, in familial cardiomyopathies, reports have demonstrated the role of defective UPS activity in the pathophysiological mechanisms. Indeed, mutations in genes encoding αB-crystallin (26) or cardiac myosin-binding protein C (27) involve cardiac UPS impairment in patients and mice (28-30).

In our study, we clearly observed major contractile dysfunction of EHT when treated with UPS inhibitor.

As for cardiac and muscular laminopathies, Kandert *et al.* reported dysfunction of the UPS associated with impairment of proliferation and differentiation capacities of myoblasts from EDMD patients expressing p.R545C lamin A/C (31). In our study, we raised the hypothesis that UPS dysfunction could be an indirect consequence of the lamin haploinsufficiency. Additionally, we showed that the sole presence of ΔK32-lamin did not lead to accumulation of ubiquitinated proteins neither in NMCM (Fig 4) nor in EHTs (Fig 6B), suggesting that UPS impairment was not triggered directly by ΔK32-lamin. Although we cannot exclude that ΔK32-lamin A/C steady-state degradation might directly overwhelm the proteolytic capacity of the UPS *in vivo*, our data suggest that UPS impairment might rather occur as a consequence of high degradation workflow imposed by cardiac remodelling in Het mice. This notion is supported by the absence of UPS dysfunction in non-pathological tissues (skeletal muscle, liver and kidney) of Het mice, indicating a cardiac-specific impairment of this system. Of note, degradation of ΔK32-lamin and UPS impairment is one of the mechanisms leading to modulation of lamin A/C expression in Het hearts, but some other processes might exist in parallel and need to be further investigated.

Even if the mechanisms leading to UPS impairment are not fully established in heart diseases, UPS is known to be essential for the balanced turnover of functionally important cardiac proteins such as contractile proteins (32), membrane receptors (33, 34), signalling pathways like NF-κB (35), β-catenin (36) or p53 (37), regulating inflammation, cardiac remodelling and apoptosis. Hence, appropriate activity of UPS is essential to maintain normal cardiac function.

Dominant negative effect of ΔK32-lamin A/C

We recently reported that homozygous *Lmna*$^{\Delta K32/\Delta K32}$ mice died at 2 weeks of age because of severe global maturation defects and metabolic disorders (16). They exhibited only ΔK32-lamin A/C in all tissues, albeit at a reduced level. Interestingly, *Lmna*$^{\Delta K32/\Delta K32}$ mice showed a more severe phenotype than *Lmna*$^{-/-}$ mice (which die at 8 weeks of age) (13) suggesting that ΔK32-lamin A/C is highly

deleterious. Dominant negative effect of ΔK32-lamin A/C is also supported by data from *C. elegans*. Indeed, Ce-ΔK46-lamin (homologous to ΔK32-lamin) filaments displayed defective lateral assembly leading to abnormal lamin network *in vitro* (38).

In the heterozygous context, we supposed that Wt and ΔK32-lamin form homodimers (Wt-Wt and ΔK32-ΔK32) as well as heterodimers (Wt-ΔK32) that further assemble into heterogeneous Wt/ ΔK32 filaments. As in *C. elegans*, the absence of lysine 32 might impact lamin filament conformation in Het mice, leading to the degradation of filaments composed by a too high proportion of ΔK32-lamin. Results obtained by mass spectrometry revealed that the ratio of ΔK32-lamin to Wt-lamin is maintained to 8% over time, suggesting that filaments composed by more than 8% of ΔK32-lamin are targeted for degradation. This hypothesis may explain the important reduction of the ΔK32-lamin but also the partially reduced pool of Wt-lamin, resulting in haploinsufficicency in the heart of 10 and 30 week-old Het mice.

The key and original finding of the present study is the altered proteasomal-mediated degradation system restricted to the heart with the course of DCM, which associates with the increase in lamin A/C amount in Het hearts. These results suggest that ΔK32-lamin A/C degradation via the UPS occurs as a protective mechanism to impede its aggregation into nuclei, as seen in EHTs.

Altogether, these observations reinforce the idea that the presence of ΔK32-lamin in the heart of Het mice may disturb correct filament assembly of Wt-lamin, leading to lamina defects. Our data further support the notion of 'toxic' effect of ΔK32-lamin A/C already observed in *Lmna*$^{\Delta K32/\Delta K32}$ mice and *C. elegans*. Further studies are needed to elucidate how ΔK32-lamin A/C exerts its negative effect, either by increasing sensitivity to mechanical stress and/or by modifying interactions with partners essential for heart function.

Conclusion

Lmna$^{\Delta K32/+}$ mice are the first knock-in *Lmna* mice associated with a cardiac-specific phenotype at the heterozygous state, and therefore recapitulate features of DCM associated with dominant A-type lamin mutations in patients. *Lmna*$^{\Delta K32/+}$ mice constitute a reliable model for further evaluations of potential

therapies of A-type lamin related-DCM. To recapitulate our findings, we propose the following sequence of events (Fig 7): (i) ΔK32-lamin A/C disturb the assembly into protofilaments and are thus targeted for degradation through the UPS. (ii) The resulting lamin A/C haploinsufficiency contributes to heart tissue vulnerability. (iii) Remodelling mechanisms counteract the higher myocardial sensitivity but have global deleterious effects including UPS function. (iv) The latter causes ΔK32-lamin A/C amount to increase, which worsens its dominant negative effect on Wt-lamin function. (v) This precipitates cardiac dysfunction and leads to congestive heart failure and death of Het mice. Overall, our findings suggest that the balance between degradation of mutant lamin to reduce its toxic effect on the one hand and global reduction in lamin A/C level (haploinsufficiency) resulting from this elimination on the other hand constitutes the major pathomechanism leading to DCM in Het mice.

MATERIALS AND METHODS

Animals

Lmna$^{\Delta K32}$ knock-in mice were generated as previously described (16). Mice were studied according to protocols approved by the European legislation (L358-86/609/EEC). We explored the cardiac phenotype of Het mice at three different ages corresponding to different stages of heart function: 10 week-old mice without any cardiac dysfunction, 30 week-old mice starting heart dysfunction and 57 week-old mice at advanced-stage of DCM (Supplemental tables 2 and 3). The Ub^{G76V}-GFP/1 mice were generated and characterized as previously described (18). They ubiquitously express a green fluorescent protein (GFP)-fused proteasome substrate.

Cardiac function measurement

Transthoracic echocardiography was performed at room temperature using an echocardiography-Doppler (General Electric Medical systems Co, Vivid 7 Dimension/Vivid 7 PRO) with a probe emitting ultrasounds with 9-14 MHz frequency. Mice were slightly anesthetized with 0.5–1% isoflurane in 100%O_2. The two-dimensionally guided Time Motion mode recording of the left ventricle (LV) provided the following measurements: interventricular septal wall thickness in diastole (IVSd), posterior wall thickness in diastole (PWd), LV end-diastolic (LVEDD) and LV end-systolic (LVESD) diameters. Each set of measurements were obtained from a same cardiac cycle. At least three sets of measures were obtained from three different cardiac cycles. LV mass (LVM) and percentage of LV Fractional Shortening (%) were calculated as follows: $[(IVSd + PWd + EDD)^3 - EDD^3] \times 1.055$ (39) and (LVEDD - LVESD)/LVEDD x100, respectively.

Electrocardiographs (ECG) were performed in conscious mice. Mice were placed in cages in a way that each limb contacted a receiver for transmission of ECG signals. ECG traces were recorded during 20 min and analysed with ECG Auto software (EMKA). QRS duration, RR and PR intervals were measured.

Production of adeno-associated virus

FLAG-tag was inserted before the ATG codon of WT- and ΔK32-human prelamin A constructs by PCR. They were subcloned into the pSMD2-CMV vector for adeno-associated virus serotype 6 (AAV-6) production as described previously (40). Virus titers ranged from $1.92x10^{12}$ to $1.03\ x10^{13}$ virus genomes/ml.

Cardiomyocytes culture and analysis

Neonatal mouse cardiac myocytes (NMCM) were isolated from C57/BL6J mice as previously described (28). NMCM were transduced with AAV-6 encoding Flag-Wt- or Flag-ΔK32-prelamin A at MOI (Multiplicity Of Infection) of 30,000. Cells were treated with 500 nM epoxomicin in 10% DMSO or with DMSO alone for 24 h. NMCM were harvested 48 h after transduction.

Engineered Heart Tissue generation and analysis

Fibrin-based engineered heart tissues (EHT) from neonatal rat heart cells were generated and cultured as previously described (19). Briefly, for each EHT, a 100 µl-reconstitution mix containing $4x10^5$ cells/EHT, bovine fibrinogen, aprotinin, and DMEM was mixed with 3 µl thrombin and pipetted around two elastic silicone posts. EHTs were transduced with AAV-6 encoding Flag-Wt- or Flag-ΔK32-prelamin A at a MOI of 1000 directly added in the reconstitution mix. At day 17, EHTs were treated with 500 nM epoxomicin in 10% DMSO or with DMSO alone for 24 h. Contraction measurements were performed by video optical recording on day 8, 11, 15, 16 and 17 as previously described (19). Average force and contraction and relaxation velocities were calculated from the recorded contractions by an algorithm that takes into account the elastic properties of the silicone posts.

Histology and immunochemical analysis

Fresh heart samples were snap frozen in liquid-nitrogen-cooled isopentane, and stored at -80°C until further processing. Frozen sections (8 µm) of transversal cardiac muscle were stained with Sirius red for fibrosis visualization. Sections were analyzed by light microscopy.

For immunohistochemical analysis, tissue sections were fixed for 10 min in 100% acetone at -20°C and incubated for 30 min with blocking solution (5% bovine serum albumin IgG-free in PBS) at room temperature. For detection of lamin A/C and lamin B, primary rabbit anti-lamin A/C polyclonal Antibody (Ab) (1:100, Santa Cruz) and primary goat anti-lamin B polyclonal Ab (1:100, Santa Cruz) were diluted in 5% bovine serum albumin IgG-free in PBS and sections were incubated for 90 min at room temperature. Sections were washed three times with PBS and incubated with secondary Ab (1:500, Alexa fluor 488 chicken anti-rabbit IgG and Alexa fluor 568 donkey anti-goat IgG) for 30 min at room temperature. Cardiac sections were mounted with mounting medium (Vectashield) with 40,6-diamidino-2-phenylindole dihydrochloride (DAPI) and images were collected with a Carl Zeiss Axiophot1 fluorescence microscope.

For immunofluorescence analysis of EHTs, the entire EHTs were analysed using confocal imaging. EHTs were rinsed with PBS and fixed with Histofix® (Roth) overnight at 4°C. The samples where then removed from the silicon post and treated 24 h with blocking solution (TBS 0.05 M, pH 7.4, 10% FCS, 1% BSA, 0.5% Triton X-100) at 4°C. Immunofluorescence was performed with mouse anti-FLAG monoclonal Ab (1:250, Sigma Aldrich) and MF20 (1:500, DSHB) and Alexa-fluor 488 anti-mouse and Alexa-fluor 546 anti-rabbit secondary Ab (1:600, Invitrogen). Nuclei were stained with DAPI. Incubation was 24 h for first and secondary antibody, respectively. Finally, the EHTs were fixed between a cover slip and a glass slide, and the fluorescence signal was analyzed using a Carl Zeiss confocal microscope (Zeiss LSM 510 META).

Electron microscopy

The ultrastructure of the myocardium of 12 mice was analysed: 6 Het and 6 WT siblings (4 at 12 weeks, 2 at 35 weeks, 2 at 51 weeks, and 4 at 67 weeks of age). Freshly harvested left ventricle apex was cut in small pieces and immediately fixed by immersion in 2.5% glutaraldehyde diluted in saline phosphate buffer (PBS) during 1 hour at room temperature. After abundant washing in PBS, samples were post-fixed with 2% OsO4, dehydrated in a graded series of acetone including a 2% uranyl acetate in 70% acetone step, and finally embedded in epoxy resin. Ultrathin sections were stained with uranyl

acetate and lead citrate, examined using a CM120 Philips transmission electron microscope and photographed with a digital SIS Morada camera, using iTEM software.

Protein analysis

For western blot analyses, proteins were extracted from frozen total heart (ventricles and atria), gastrocnemius muscle, liver and kidney as previously described (16). Total proteins were separated by SDS–PAGE and hybridized with primary rabbit anti-lamin A/C polyclonal Ab (1:2000, Santa Cruz), primary rabbit anti-emerin polyclonal Ab (1:1000, kindly provided by G.E. Morris, NEWI, UK), primary rabbit anti-actin polyclonal Ab (1:1000, Sigma Aldrich), mouse anti-ubiquitinated monoclonal Ab (1:5000, Enzo Lifesciences), mouse anti-FLAG-M2 monoclonal Ab (1:1000, Sigma Aldrich), mouse anti-vinculin monoclonal Ab (1:1000, Sigma Aldrich) or rabbit anti-GFP polyclonal Ab (1:1000, AbCam) and with secondary rabbit anti-mouse (for monoclonal Ab) or goat anti-rabbit (for polyclonal Ab) IgG HRP-conjugated Ab (1:2000, Dako A/S). Recognized proteins were visualized by enhanced chemiluminescence (Pierce or Millipore). Hybridization signals were quantified using MultiGauge software and normalized to actin, vinculin or Ponceau staining.

LC-MS/MS analysis

Heart protein extracts for mass spectrometry (MS) analysis were prepared as described in the Western blotting procedure (Supplemental methods) and separated using SDS-PAGE. The gel lanes containing the lamin A and lamin C proteins were cut out and digested separately using in-gel tryptic digestion as previously described (41). Briefly, the gel bands were shrunk using acetonitrile, in-gel reduced and alkylated followed by saturation of the gel pieces with trypsin. Digestion was performed overnight at 37°C. The resulting peptides were desalted using in-house made StageTips as previously described (42) and analyzed by a nanoLC-MS/MS system (LTQ-Orbitrap XL, Thermo Fisher Scientific). The peptides were eluted from an in-house packed fused-silica (length: 20 cm; i.d. 75 µm) reversed-phase column (3 µm C18, ReproSil-Pur C18 AQ, Dr. Maisch, Germany) using an 80% acetonitrile (ACN), 0.5% acetic acid gradient, starting with 2% ACN and ending with 80% ACN. The MS full scans were detected in the Orbitrap, with MS/MS scans being detected in the LTQ iontrap. The peptides were

identified by searching tandem MS spectra using the Mascot search engine (Matrix Science) against a custom-made mouse database, containing the sequence of the ΔK32 variant (Uniprot release 2011_01, restricted to UniProtKB/Swiss-Prot and Taxonomy: *mus musculus* (mouse) (49954 sequences)). The label-free quantification was performed using two different approaches: i) MaxQuant's intensity-based label-free quantification where total peptide signals were determined in the mass-to-charge, elution time and intensity space (43 , 44) and ii) integration of peptide extracted ion-chromatograms using the ICIS integration algorithms in the Qual browser program (Thermo Fisher Scientific) (45). Details and validation of the label free quantification approach is provided in Supplemental Figure 4A and 4B.

mRNA analysis

Hearts were dissected and rapidly frozen in liquid-nitrogen. Total RNA extraction and Q-PCR were performed as previously described (16). Individual expression values were normalized by comparison with *Rplp0* mRNA, encoding ribosomal protein large P0. The sequences of oligonucleotides used for Q-PCR analysis are listed into supplemental table 4. *Lmna* expression level was measured using oligonucleotides matching with a common region of Wt and mutant on the cDNA. *Lmna Wt* and *ΔK32* expression level, encoding Wt and mutant lamin A/C protein respectively, were measured using hydrolysis probe technique. Hydrolysis probes were designed to match specifically with Wt or deleted nucleotide region of *Lmna* cDNA with LightCycler 480 Probes Master kit (Roche Diagnostic).

Skeletal muscle analysis

Spontaneous activity and immunostaining were performed as previously described (4646). The morphology of the *gastrocnemius* muscle was analysed blindly by the histopathologists from the Myology Institute. For measurement of isometric contractile properties of muscles, after removal, muscles were soaked in an oxygenated Krebs solution (95% O_2 and 5% CO_2) containing 58.5 mM NaCl, 24 mM $NaHCO_3$, 5.4 mM KCl, 1.2 mM KH_2PO_4, 1.8 mM $CaCl_2$, 1 mM $MgSO_4$, and 10 mM glucose, pH 7.4, and maintained at a temperature of 22°C. One of the muscle tendons was attached to a lever arm of a servomotor system (300B Dual-Mode Lever; Aurora Scientific). After equilibration (30 min), electrical stimulation was delivered through electrodes running parallel to the muscle. 1 ms

pulses were generated by a high power stimulator (701B; Aurora Scientific). P_0 was measured at L_0 during isometric contractions in response to electrical stimulation (frequency of 50–125 Hz; train of stimulation of 1500 ms). Time to peak and time to half relaxation were recorded. Muscles were weighted and the specific force IsoN was calculated by dividing P_0 by muscle weigh.

Statistical analysis

Differences between groups were assessed using ANOVA and Student's t-test with Sigmastat software. Values of $p<0.05$ were considered statistically significant.

ACKNOWLEDGEMENTS

We thank C. Enond and her team at the Animal facility of Pitié-Salpêtrière campus (Centre d'Expérimentation Fonctionnelle, Faculté de Médecine Pierre Marie Curie) for her work and help in the mouse colony maintenance; B. Geertz (Hamburg) and A. Jacquet (Paris) for echocardiography, S. Bouyon for ECG analysis, N. Guerchet, F. Fougerousse and G. Tanniou for muscle analysis, C. Beley, G. Précigout, L. Garcia for AAV production, N. Dantuma (Stockholm, Sweden) for providing Ub^{G76V}-GFP transgenic mice, and finally V. Allamand, C. Coirault, and T. Voit for critical reading and fruitful discussion. The monoclonal antibody against myosin (MF20) developed by Fishman, D.A. was obtained from the DSHB developed under the auspices of the NICHD and maintained by The University of Iowa, Department of Biology, Iowa City, IA 52242.

CONFLICTS OF INTEREST STATEMENT:

None to declare.

FUNDINGS

This work was financially supported by the *Institut National de la Santé et de la Recherche Médicale*; the *Université Pierre et Marie Curie Paris 06*, the *Centre National de la Recherche Scientifique*; the *Association Française contre les Myopathies*; the sixth and seventh Framework Programs of the European Union (Euro-laminopathies #018690, Marie Curie EXT-014051; Health-F2-2009-241577-Big-Heart project), the Deutsche Forschungsgemeinschaft (FOR-604-CA 618/1-1 and 1-2), and the Leducq Foundation (Research grant Nr. 11, CVD 04).

REFERENCES

1. Hershberger, R. E., and Siegfried, J. D. (2011) Update 2011: clinical and genetic issues in familial dilated cardiomyopathy. *J. Am. Coll. Cardiol.* **57**, 1641-1649
2. Ben Yaou, R., Gueneau, L., Demay, L., Stora, S., Chikhaoui, K., Richard, P., and Bonne, G. (2006) Heart involvement in lamin A/C related diseases. *Arch. Mal. Coeur Vaiss.* **99**, 848-855
3. Fatkin, D., MacRae, C., Sasaki, T., Wolff, M. R., Porcu, M., Frenneaux, M., Atherton, J., Vidaillet, H. J., Jr., Spudich, S., De Girolami, et al. (1999) Missense mutations in the rod domain of the lamin A/C gene as causes of dilated cardiomyopathy and conduction-system disease. *N. Engl. J. Med.* **341**, 1715-1724
4. Worman, H. J., and Bonne, G. (2007) "Laminopathies": a wide spectrum of human diseases. *Exp. Cell. Res.* **313**, 2121-2133
5. Quijano-Roy, S., Mbieleu, B., Bonnemann, C. G., Jeannet, P. Y., Colomer, J., Clarke, N. F., Cuisset, J. M., Roper, H., De Meirleir, L., D'Amico, A., et al. (2008) De novo LMNA mutations cause a new form of congenital muscular dystrophy. *Ann. Neurol.* **64**, 177-186
6. Bonne, G., Di Barletta, M. R., Varnous, S., Becane, H. M., Hammouda, E. H., Merlini, L., Muntoni, F., Greenberg, C. R., Gary, F., Urtizberea, J. A., et al. (1999) Mutations in the gene encoding lamin A/C cause autosomal dominant Emery-Dreifuss muscular dystrophy. *Nat. Genet.* **21**, 285-288
7. Muchir, A., Bonne, G., van der Kooi, A. J., van Meegen, M., Baas, F., Bolhuis, P. A., de Visser, M., and Schwartz, K. (2000) Identification of mutations in the gene encoding lamins A/C in autosomal dominant limb girdle muscular dystrophy with atrioventricular conduction disturbances (LGMD1B). *Hum. Mol. Genet.* **9**, 1453-1459

8. Lin, F., and Worman, H. J. (1993) Structural organization of the human gene encoding nuclear lamin A and nuclear lamin C. *J. Biol. Chem*. **268**, 16321-16326

9. Broers, J. L., Ramaekers, F. C., Bonne, G., Yaou, R. B., and Hutchison, C. J. (2006) Nuclear lamins: laminopathies and their role in premature ageing. *Physiol. Rev.* **86**, 967-1008

10. Schirmer, E. C., and Foisner, R. (2007) Proteins that associate with lamins: many faces, many functions. *Exp. Cell. Res.* **313**, 2167-2179

11. Favreau, C., Dubosclard, E., Ostlund, C., Vigouroux, C., Capeau, J., Wehnert, M., Higuet, D., Worman, H. J., Courvalin, J. C., and Buendia, B. (2003) Expression of lamin A mutated in the carboxyl-terminal tail generates an aberrant nuclear phenotype similar to that observed in cells from patients with Dunnigan-type partial lipodystrophy and Emery-Dreifuss muscular dystrophy. *Exp. Cell. Res.* **282**, 14-23

12. Wang, Y., Herron, A. J., and Worman, H. J. (2006) Pathology and nuclear abnormalities in hearts of transgenic mice expressing M371K lamin A encoded by an LMNA mutation causing Emery-Dreifuss muscular dystrophy. *Hum. Mol. Genet.* **15**, 2479-2489

13. Nikolova, V., Leimena, C., McMahon, A. C., Tan, J. C., Chandar, S., Jogia, D., Kesteven, S. H., Michalicek, J., Otway, R., Verheyen, F., et al. (2004) Defects in nuclear structure and function promote dilated cardiomyopathy in lamin A/C-deficient mice. *J. Clin. Invest.* **113**, 357-369

14. Wolf, C. M., Wang, L., Alcalai, R., Pizard, A., Burgon, P. G., Ahmad, F., Sherwood, M., Branco, D. M., Wakimoto, H., Fishman, G. I., et al. (2008) Lamin A/C haploinsufficiency causes dilated cardiomyopathy and apoptosis-triggered cardiac conduction system disease. *J. Mol. Cell. Cardiol.* **44**, 293-303

15. Chandar, S., Yeo, L. S., Leimena, C., Tan, J. C., Xiao, X. H., Nikolova-Krstevski, V., Yasuoka, Y., Gardiner-Garden, M., Wu, J., Kesteven, S., et al. (2010) Effects of mechanical stress and carvedilol in lamin A/C-deficient dilated cardiomyopathy. *Circ. Res.* **106**, 573-582

16. Bertrand, A. T., Renou, L., Papadopoulos, A., Beuvin, M., Lacene, E., Massart, C., Ottolenghi, C., Decostre, V., Maron, S., Schlossarek, S., et al. (2012) DelK32-lamin A/C has abnormal location and induces incomplete tissue maturation and severe metabolic defects leading to premature death. *Hum. Mol. Genet.* **21**, 1037-1048

17. Rock, K. L., Gramm, C., Rothstein, L., Clark, K., Stein, R., Dick, L., Hwang, D., and Goldberg, A. L. (1994) Inhibitors of the proteasome block the degradation of most cell proteins and the generation of peptides presented on MHC class I molecules. *Cell* **78**, 761-771

18. Lindsten, K., Menendez-Benito, V., Masucci, M. G., and Dantuma, N. P. (2003) A transgenic mouse model of the ubiquitin/proteasome system. *Nat. Biotechnol.* **21**, 897-902

19. Hansen, A., Eder, A., Bonstrup, M., Flato, M., Mewe, M., Schaaf, S., Aksehirlioglu, B., Schwoerer, A. P., Uebeler, J., and Eschenhagen, T. (2010) Development of a drug screening platform based on engineered heart tissue. *Circ. Res.* **107**, 35-44

20. Becane, H. M., Bonne, G., Varnous, S., Muchir, A., Ortega, V., Hammouda, E. H., Urtizberea, J. A., Lavergne, T., Fardeau, M., Eymard, B., et al. (2000) High incidence of sudden death with conduction system and myocardial disease due to lamins A and C gene mutation. *Pacing Clin. Electrophysiol.* **23**, 1661-1666

21. van Tintelen, J. P., Tio, R. A., Kerstjens-Frederikse, W. S., van Berlo, J. H., Boven, L. G., Suurmeijer, A. J., White, S. J., den Dunnen, J. T., te Meerman, G. J., Vos, Y. J., et

al. (2007) Severe myocardial fibrosis caused by a deletion of the 5' end of the lamin A/C gene. *J. Am. Coll. Cardiol.* **49**, 2430-2439

22. Pasotti, M., Klersy, C., Pilotto, A., Marziliano, N., Rapezzi, C., Serio, A., Mannarino, S., Gambarin, F., Favalli, V., Grasso, M., et al. (2008) Long-term outcome and risk stratification in dilated cardiolaminopathies. *J. Am. Coll. Cardiol* .**52**, 1250-1260

23. Gupta, P., Bilinska, Z. T., Sylvius, N., Boudreau, E., Veinot, J. P., Labib, S., Bolongo, P. M., Hamza, A., Jackson, T., Ploski, R., et al.. (2010) Genetic and ultrastructural studies in dilated cardiomyopathy patients: a large deletion in the lamin A/C gene is associated with cardiomyocyte nuclear envelope disruption. *Basic Res. Cardiol.* **105**, 365-377

24. Jahn, D., Schramm, S., Schnolzer, M., Heilmann, C. J., de Koster, C. G., Schutz, W., Benavente, R., and Alsheimer, M. (2012) A truncated lamin A in the Lmna (-/-) mouse line: Implications for the understanding of laminopathies. *Nucleus* **3,** 463-474

25. Schlossarek, S., and Carrier, L. (2011) The ubiquitin-proteasome system in cardiomyopathies. *Curr. Opin. Cardiol.* **26**, 190-195

26. Vicart, P., Caron, A., Guicheney, P., Li, Z., Prevost, M. C., Faure, A., Chateau, D., Chapon, F., Tome, F., Dupret, J. M., et al. (1998) A missense mutation in the alphaB-crystallin chaperone gene causes a desmin-related myopathy. *Nat. Genet.* **20**, 92-95

27. Richard, P., Charron, P., Carrier, L., Ledeuil, C., Cheav, T., Pichereau, C., Benaiche, A., Isnard, R., Dubourg, O., Burban, M., et al. (2003) Hypertrophic cardiomyopathy: distribution of disease genes, spectrum of mutations, and implications for a molecular diagnosis strategy. *Circulation* **107**, 2227-2232

28. Vignier, N., Schlossarek, S., Fraysse, B., Mearini, G., Kramer, E., Pointu, H., Mougenot, N., Guiard, J., Reimer, R., Hohenberg, H., et al. (2009) Nonsense-mediated

mRNA decay and ubiquitin-proteasome system regulate cardiac myosin-binding protein C mutant levels in cardiomyopathic mice. *Circ. Res.* **105**, 239-248

29. Liu, J., Chen, Q., Huang, W., Horak, K. M., Zheng, H., Mestril, R., and Wang, X. (2006) Impairment of the ubiquitin-proteasome system in desminopathy mouse hearts. *FASEB J.* **20**, 362-364

30. Sanbe, A., Osinska, H., Saffitz, J. E., Glabe, C. G., Kayed, R., Maloyan, A., and Robbins, J. (2004) Desmin-related cardiomyopathy in transgenic mice: a cardiac amyloidosis. *Proc. Natl. Acad. Sci. U. S. A.* **101**, 10132-10136

31. Kandert, S., Wehnert, M., Muller, C. R., Buendia, B., and Dabauvalle, M. C. (2009) Impaired nuclear functions lead to increased senescence and inefficient differentiation in human myoblasts with a dominant p.R545C mutation in the LMNA gene. *Eur. J. Cell. Biol.* **88**, 593-608

32. Eble, D. M., Spragia, M. L., Ferguson, A. G., and Samarel, A. M. (1999) Sarcomeric myosin heavy chain is degraded by the proteasome. *Cell. Tissue Res* .**296**, 541-548

33. Shenoy, S. K., McDonald, P. H., Kohout, T. A., and Lefkowitz, R. J. (2001) Regulation of receptor fate by ubiquitination of activated beta 2-adrenergic receptor and beta-arrestin. *Science* **294**, 1307-1313

34. Penela, P., Ruiz-Gomez, A., Castano, J. G., and Mayor, F., Jr. (1998) Degradation of the G protein-coupled receptor kinase 2 by the proteasome pathway. *J. Biol. Chem.* **273**, 35238-35244

35. Skaug, B., Jiang, X., and Chen, Z. J. (2009) The role of ubiquitin in NF-kappaB regulatory pathways. *Annu. Rev. Biochem.* **78**, 769-796

36. Aberle, H., Bauer, A., Stappert, J., Kispert, A., and Kemler, R. (1997) beta-catenin is a target for the ubiquitin-proteasome pathway. *EMBO J.* **16**, 3797-3804

37. Birks, E. J., Latif, N., Enesa, K., Folkvang, T., Luong le, A., Sarathchandra, P., Khan, M., Ovaa, H., Terracciano, C. M., Barton, P. J., et al. (2008) Elevated p53 expression is associated with dysregulation of the ubiquitin-proteasome system in dilated cardiomyopathy. *Cardiovasc. Res.* **79**, 472-480

38. Bank, E. M., Ben-Harush, K., Wiesel-Motiuk, N., Barkan, R., Feinstein, N., Lotan, O., Medalia, O., and Gruenbaum, Y. (2011) A laminopathic mutation disrupting lamin filament assembly causes disease-like phenotypes in Caenorhabditis elegans. *Mol. Biol. Cell* **22**, 2716-2728

39. Tanaka, N., Dalton, N., Mao, L., Rockman, H. A., Peterson, K. L., Gottshall, K. R., Hunter, J. J., Chien, K. R., and Ross, J., Jr. (1996) Transthoracic echocardiography in models of cardiac disease in the mouse. *Circulation* **94**, 1109-1117

40. Riviere, C., Danos, O., and Douar, A. M. (2006) Long-term expression and repeated administration of AAV type 1, 2 and 5 vectors in skeletal muscle of immunocompetent adult mice. *Gene Ther.* **13**, 1300-1308

41. Shevchenko, A., Tomas, H., Havlis, J., Olsen, J. V., and Mann, M. (2006) In-gel digestion for mass spectrometric characterization of proteins and proteomes. *Nat. Protoc.* **1**, 2856-2860

42. Rappsilber, J., Mann, M., and Ishihama, Y. (2007) Protocol for micro-purification, enrichment, pre-fractionation and storage of peptides for proteomics using StageTips. *Nat. Protoc.* **2**, 1896-1906

43. Cox, J., and Mann, M. (2008) MaxQuant enables high peptide identification rates, individualized p.p.b.-range mass accuracies and proteome-wide protein quantification. *Nat. Biotech.***26**, 1367-1372

44. Luber, C. A., Cox, J., Lauterbach, H., Fancke, B., Selbach, M., Tschopp, J., Akira, S., Wiegand, M., Hochrein, H., O'Keeffe, M., et al. (2010) Quantitative proteomics reveals subset-specific viral recognition in dendritic cells. *Immunity* **32**, 279-289

45. Hansen, J., Corydon, T. J., Palmfeldt, J., Durr, A., Fontaine, B., Nielsen, M. N., Christensen, J. H., Gregersen, N., and Bross, P. (2008) Decreased expression of the mitochondrial matrix proteases Lon and ClpP in cells from a patient with hereditary spastic paraplegia (SPG13). *Neuroscience* **153**, 474-482

46. Arimura, T., Helbling-Leclerc, A., Massart, C., Varnous, S., Niel, F., Lacene, E., Fromes, Y., Toussaint, M., Mura, A. M., Keller, D. I., et al. (2005) Mouse model carrying H222P-Lmna mutation develops muscular dystrophy and dilated cardiomyopathy similar to human striated muscle laminopathies. *Hum. Mol. Genet*. **14**, 155-169

LEGENDS TO FIGURES

Figure 1. Cardiac phenotype of Het mice.

(A) Survival curve of Wt (57 males, 58 females) and Het (51 males, 48 females) mice. (B-C) Serial echocardiography from 12 weeks of age until death in males and females Wt (n=6 per gender) and Het (n=9 per gender) mice. (B) Fractional shortening. (C) Left ventricular end-diastolic diameter. *p<0.05, **p<0.01 compared with age- and gender-matched Wt. Mean±SD. (D) Heart weight (HW) to tibia length (TL) ratio in Wt and Het mice. (n=6-17 per group) *p<0.05 **p<0.01 compared to age-matched Wt. Mean±SEM. (E) Lung weight (LW) to TL ratio in Wt and Het mice (n=6-17 per group) *p<0.05 **p<0.01 compared to age-matched Wt. Mean±SEM. (F) Expression of cardiac remodelling mRNA markers *Nppa*, *Nppb* and *Myh7* in 10 and 57 week-old Wt and Het mice (n=5-6 per group). *p<0.05, **p<0.01 compared with age-matched Wt. Mean±SEM. (G) Coronal section of Wt and Het hearts at 57 weeks of age (bar = 5 mm). (H) Cross-section of Wt and Het hearts at 57 weeks of age stained with Sirius Red (RV = right ventricle, LV = left ventricle, bar = 100 µm). (I) Proportion of fibrosis normalized to total cardiac area of 57 week-old mice (n=6 per group). *p<0.05 compared to Wt. Mean±SD.

Figure 2. Lamin A/C localization and nuclear morphology in Wt and Het hearts.

(A-C) Lamin A/C staining in Wt and Het hearts before (10 weeks, A), at early-stage (30 weeks, B) and at end-stage of DCM (57 weeks, C). Nuclei are counterstained with DAPI (bar = 10µm).

(D-H) Ultrastructural features of myocardial nuclei of 12 week-old Wt (D) and Het (E) mice and 26 week-old Het mice (F-H). Widened nuclear intermembrane space (inset 2E compared with 2D, and G, arrows), large vacuoles surrounding the nucleus (F, asterisks), nuclear membrane rupture and chromatin exit (H, arrows) (bar = 2 µm and 500 nm in insets).

Figure 3. Evolution of mutant lamin A/C expression.

(A-B) Lamin A and C, emerin protein levels in the heart of 10, 30 and 57 week-old Het and Wt mice. Actin is used as loading control. Representative blots (A) and quantification (B) of total lamin A (LaA) and C (LaC). (n=6-9 per group). ** $p<0.01$ compared to Wt. Mean±SEM. (C) Correlation between the lamin A protein level and fractional shortening in Het mice at the 3 ages. (D) Ratio of mutant ΔK32-lamin A/C to total lamin A/C quantified by mass spectrometry based label-free quantification in the heart of 10 and 57 week-old Het mice (n=7-9 per group). Mean±SEM. (E) Level of total *Lmna* mRNA in the heart of 10, 30 and 57 week-old Het and Wt mice (n=5-6 per group). Mean±SEM. (F) Ratio of specific allele level in the heart of 10, 30 and 57 week-old Het mice. Wt allele = *Lmna* Wt, mutant allele = *Lmna* ΔK32.

Figure 4. Effect of UPS inhibition on ΔK32-lamin A/C expression in neonatal mouse cardiomyocytes.

Ubiquitinated proteins, Flag-prelamin A and Flag-lamin A protein levels in untransduced (Ctl), Flag-Wt- (Wt) or Flag-ΔK32-lamin A (ΔK32) transduced NMCM treated with epoxomicin (epoxo) or DMSO as vehicle control. Vinculin was used as loading control.

Figure 5. Global impairment of UPS in the heart of Het/Ub-GFP crossed mice.

(A) Western blots showing Ub-GFP, lamin A/C and Ponceau staining from heart of 10 and 30 week-old Wt/Ub-GFP and Het/Ub-GFP mice. (B-C) Quantification of Ub-GFP protein level (B), lamin A (LaA) and C (LaC) protein level (C). *$p<0.05$, ** $p<0.01$ Mean±SEM. Value are normalized to age-matched Wt/Ub-GFP (n=8-3 per group).

Figure 6. Effect of UPS inhibition and mutant lamin A/C overexpression on rat engineered heart tissue.

(A) Force of contraction of untransduced (Control; grey bars), Flag-Wt-lamin A (Wt; black bars) or Flag-ΔK32-lamin A (ΔK32; red bars) transduced EHTs after treatment with epoxomicin (epoxo; hatched bars) or DMSO (solid bars) as vehicle . ***$p<0.001$ between before and after DMSO or epoxo

treatment. Mean±SEM (n=5-6 per group). (B) Representative western blot showing ubiquitinated proteins, Flag-prelamin A and Flag-lamin A protein levels in control, Wt and ΔK32 EHTs, treated with epoxomicin (epoxo) or DMSO as vehicle. Actin is used as loading control. (C) Immunostaining with anti-myosin heavy chain (red) and anti-Flag (green) antibodies. Nuclei are counterstained with DAPI (bar = 20µm).

Figure 7. Schematic model of pathophysiological mechanisms linking ΔK32 lamin A/C to DCM.

(A) Chronology of pathological events occurring in the heart of Het mice. (B) Working model suggesting that ΔK32 lamin A/C might disturb the assembly into protofilaments and thus be targeted for degradation (alone and/or associated to Wt lamin). It results in haploinsufficiency likely contributing to myocardial vulnerability, promoting remodelling mechanisms. These processes might have global deleterious effects, as UPS impairment. Wt and ΔK32-lamin A/C amount then increases, playing additional negative effects on cardiomyocytes function. This might precipitate cardiac dysfunction and UPS dysfunction (?), leading to DCM.

ABBREVIATIONS

AAV: Adeno-associated virus

DCM: Dilated cardiomyopathy

DCM-CD: Dilated cardiomyopathy with conduction disease

EDMD: Emery-Dreifuss muscular dystrophy

EHT: Engineered heart tissue

Het: Heterozygous *Lmna*$^{\Delta K32}$ knock-in mice

LMNA: Lamin A/C gene

MOI: Multiplicity of infection

NMCM: Neonatal mouse cardiomyocytes

Ub-GFP: mutant ubiquitin-coupled green fluorescent protein

UPS: Ubiquitin-proteasome system

Wt: Wild-type mice

Figure 1.

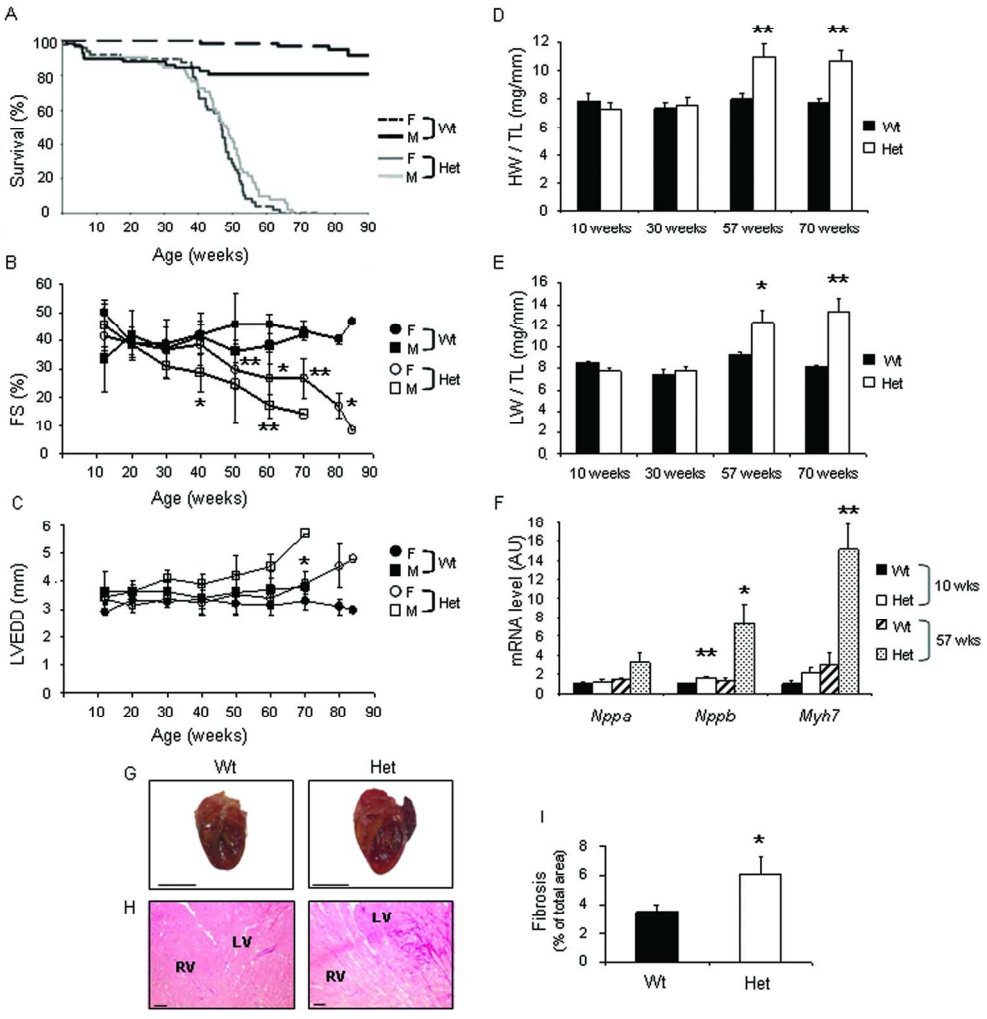

Figure 1. Cardiac phenotype of Het mice.

(A) Survival curve of Wt (57 males, 58 females) and Het (51 males, 48 females) mice. (B-C) Serial echocardiography from 12 weeks of age until death in males and females Wt (n=6 per gender) and Het (n=9 per gender) mice. (B) Fractional shortening. (C) Left ventricular end-diastolic diameter. *p<0.05, **p<0.01 compared with age- and gender-matched Wt. Mean±SD. (D) Heart weight (HW) to tibia length (TL) ratio in Wt and Het mice. (E) Lung weight (LW) to TL ratio in Wt and Het mice (n=6-17 per group) *p<0.05 **p<0.01 compared with age-matched Wt. Mean±SEM. (F) Expression of cardiac remodelling mRNA markers *Nppa, Nppb* and *Myh7* in 10 and 57 week-old Wt and Het mice (n=5-6 per group). *p<0.05, **p<0.01 compared with age-matched Wt. Mean±SEM. (G) Coronal section of Wt and Het hearts at 57 weeks of age (bar = 5 mm). (H) Cross-section of Wt and Het hearts at 57 weeks of age stained with Sirius Red (RV = right ventricle, LV = left ventricle, bar = 100 μm). (I) Proportion of fibrosis normalized to total cardiac area of 57 week-old mice (n=6 per group). *p<0.05 compared with Wt. Mean±SD.

180x193mm (300 x 300 DPI)

Figure 2.

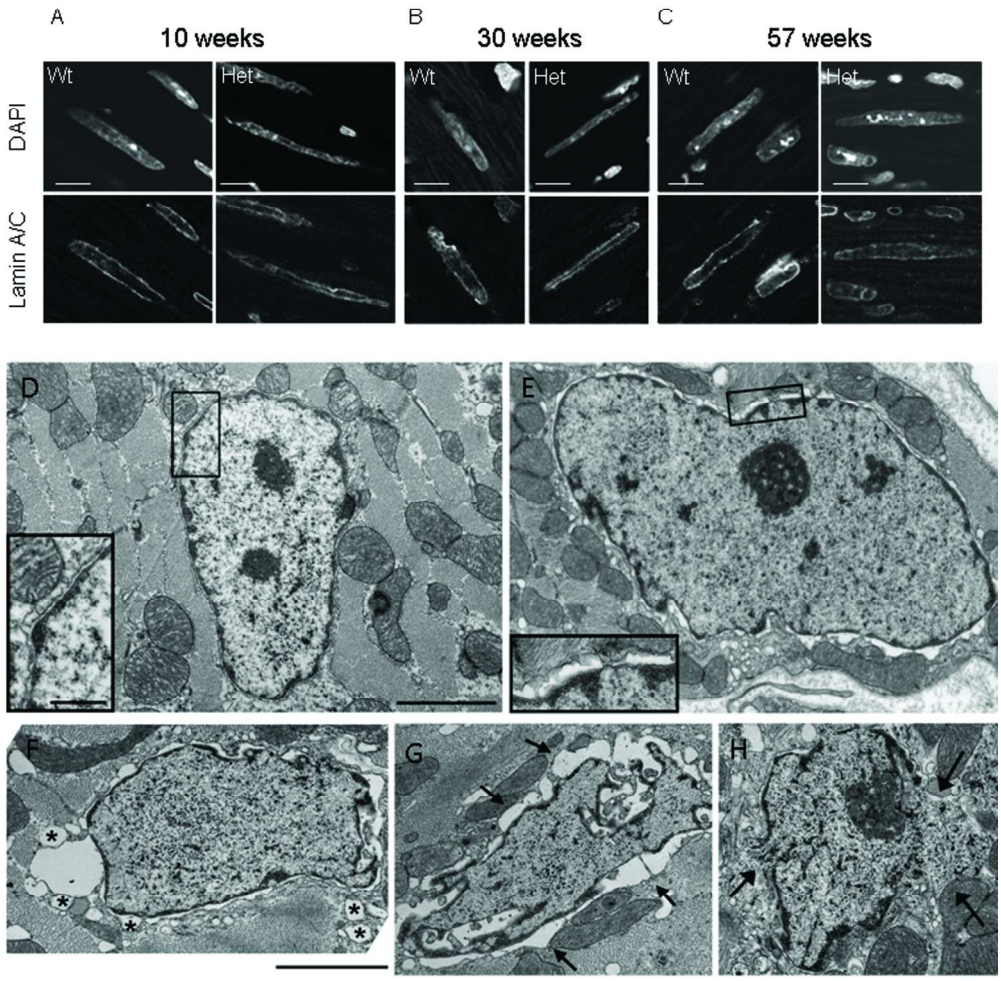

Figure 2. Lamin A/C localization and nuclear morphology in Wt and Het hearts.
(A-C) Lamin A/C staining in Wt and Het hearts before (10 weeks, A), at early-stage (30 weeks, B) and at end-stage of DCM (57 weeks, C). Nuclei are counterstained with DAPI (bar = 10µm).
(D-H) Ultrastructural features of myocardial nuclei of 12 week-old Wt (D) and Het (E) mice and 26 week-old Het mice (F-H). Widened nuclear intermembrane space (inset 2E compared with 2D, and G, arrows), large vacuoles surrounding the nucleus (F, asterisks), nuclear membrane rupture and chromatin exit (H, arrows) (bar = 2 µm and 500 nm in insets).

180x193mm (300 x 300 DPI)

Figure 3.

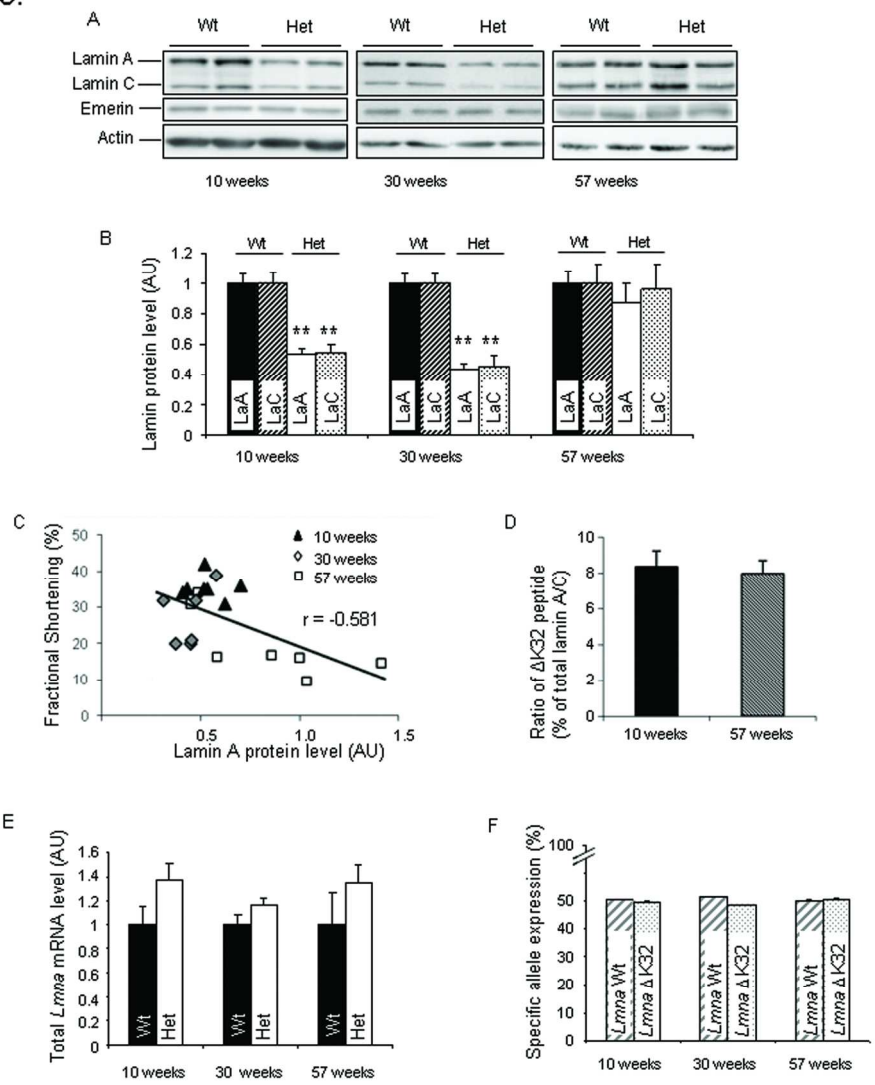

Figure 3. Evolution of mutant lamin A/C expression.

(A-B) Lamin A and C, emerin protein levels in the heart of 10, 30 and 57 week-old Het and Wt mice. Actin is used as loading control. Representative blots (A) and quantification (B) of total lamin A (LaA) and C (LaC). (n=6-9 per group). ** $p<0.01$ compared with Wt. Mean±SEM. (C) Correlation between the lamin A protein level and fractional shortening in Het mice at the 3 ages. (D) Ratio of mutant ΔK32-lamin A/C to total lamin A/C quantified by mass spectrometry based label-free quantification in the heart of 10 and 57 week-old Het mice (n=7-9 per group). Mean±SEM. (E) Level of total *Lmna* mRNA in the heart of 10, 30 and 57 week-old Het and Wt mice (n=5-6 per group). Mean±SEM. (F) Ratio of specific allele level in the heart of 10, 30 and 57 week-old Het mice. Wt allele = *Lmna* Wt, mutant allele = *Lmna* ΔK32.

180x201mm (300 x 300 DPI)

Figure 4.

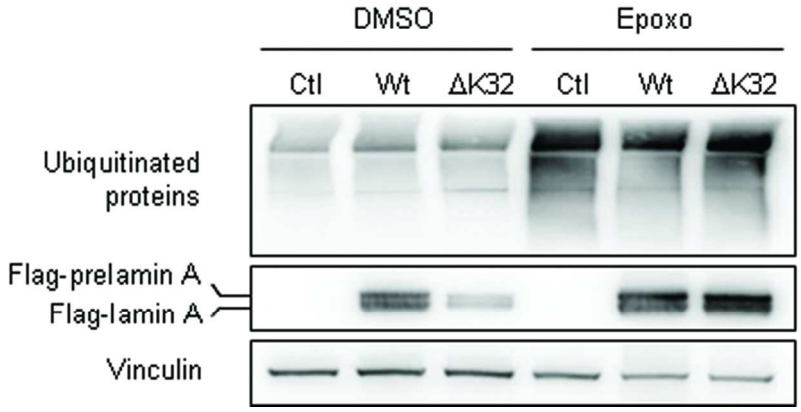

Figure 4. Effect of UPS inhibition on ΔK32-lamin A/C expression in neonatal mouse cardiomyocytes.

Ubiquitinated proteins, Flag-prelamin A and Flag-lamin A protein levels in untransduced (Ctl), Flag-Wt- (Wt) or Flag-ΔK32-lamin A (ΔK32) transduced NMCM treated with epoxomicin (epoxo) or DMSO as vehicle control. Vinculin was used as loading control.

99x47mm (300 x 300 DPI)

Figure 5.

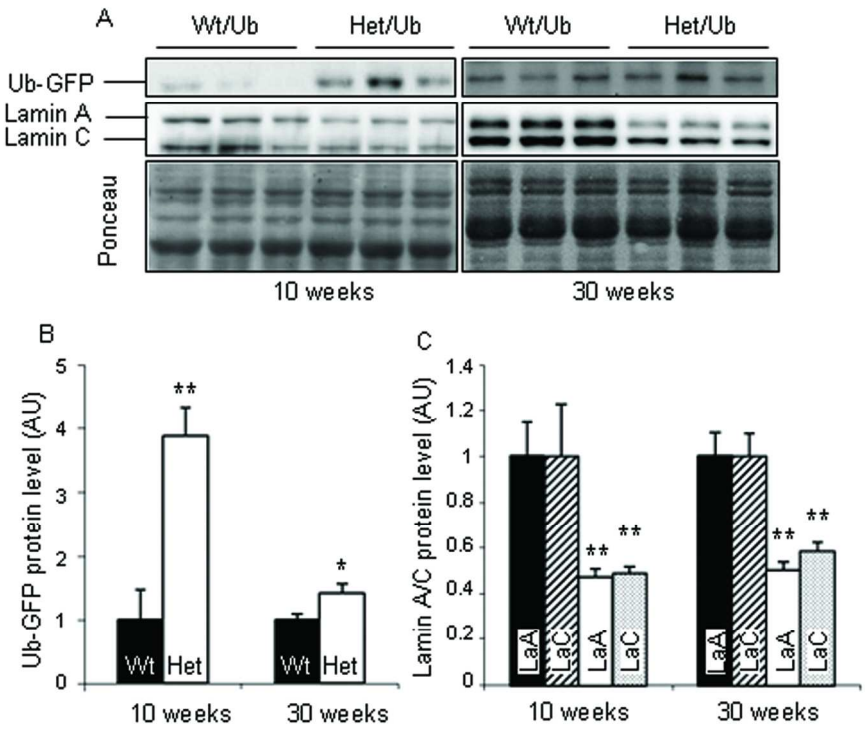

Figure 5. Global impairment of UPS in the heart of Het/Ub-GFP crossed mice.
(A) Western blots showing Ub-GFP, lamin A/C and Ponceau staining from heart of 10 and 30 week-old Wt/Ub-GFP and Het/Ub-GFP mice. (B-C) Quantification of Ub-GFP protein level (B), lamin A (LaA) and C (LaC) protein level (C). *p<0.05, ** p<0.01 Mean±SEM. Value are normalized to age-matched Wt/Ub-GFP (n=8-3 per group).

180x152mm (300 x 300 DPI)

Figure 6.

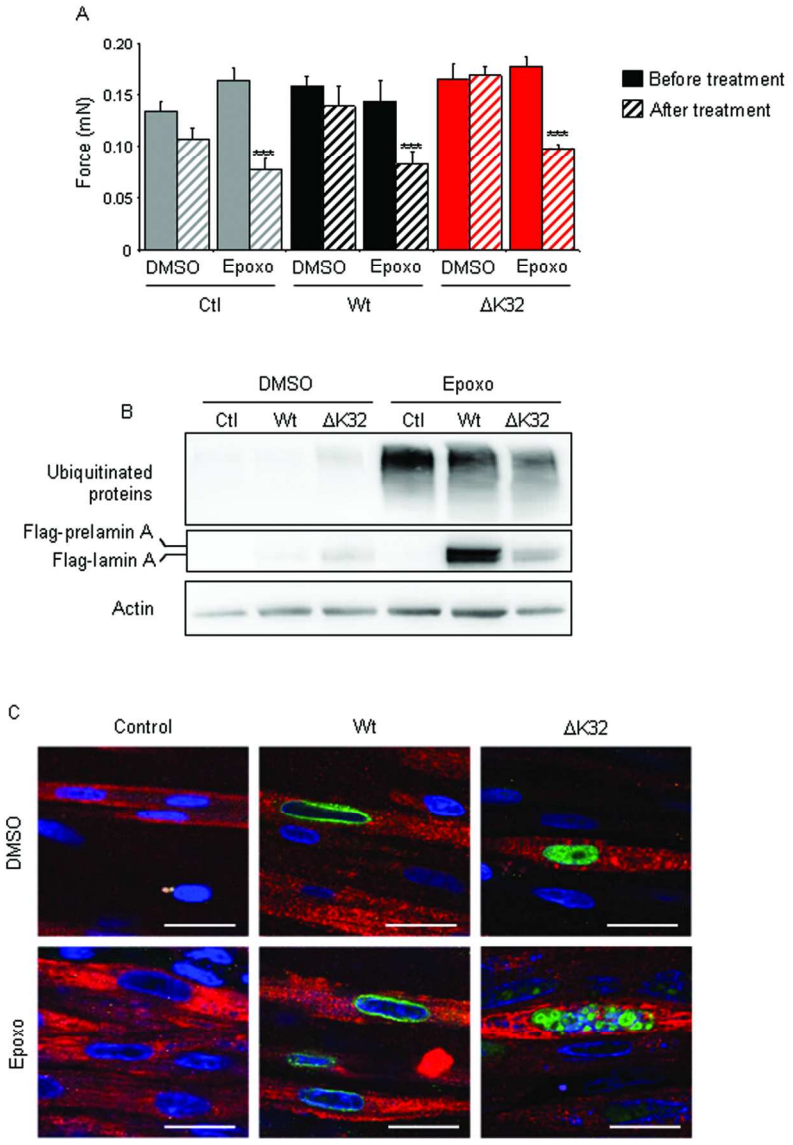

Figure 6. Effect of UPS inhibition and mutant lamin A/C overexpression on rat engineered heart tissue.

(A) Force of contraction of untransduced (Control; grey bars), Flag-Wt-lamin A (Wt; black bars) or Flag-ΔK32-lamin A (ΔK32; red bars) transduced EHTs after treatment with epoxomicin (epoxo; hatched bars) or DMSO (solid bars) as vehicle . ***p<0.001 between before and after DMSO or epoxo treatment. Mean±SEM (n=5-6 per group). (B) Representative western blot showing ubiquitinated proteins, Flag-prelamin A and Flag-lamin A protein levels in control, Wt and ΔK32 EHTs, treated with epoxomicin (epoxo) or DMSO as vehicle. Actin is used as loading control. (C) Immunostaining with anti-myosin heavy chain (red) and anti-Flag (green) antibodies. Nuclei are counterstained with DAPI (bar = 20μm).

180x220mm (300 x 300 DPI)

Figure 7.

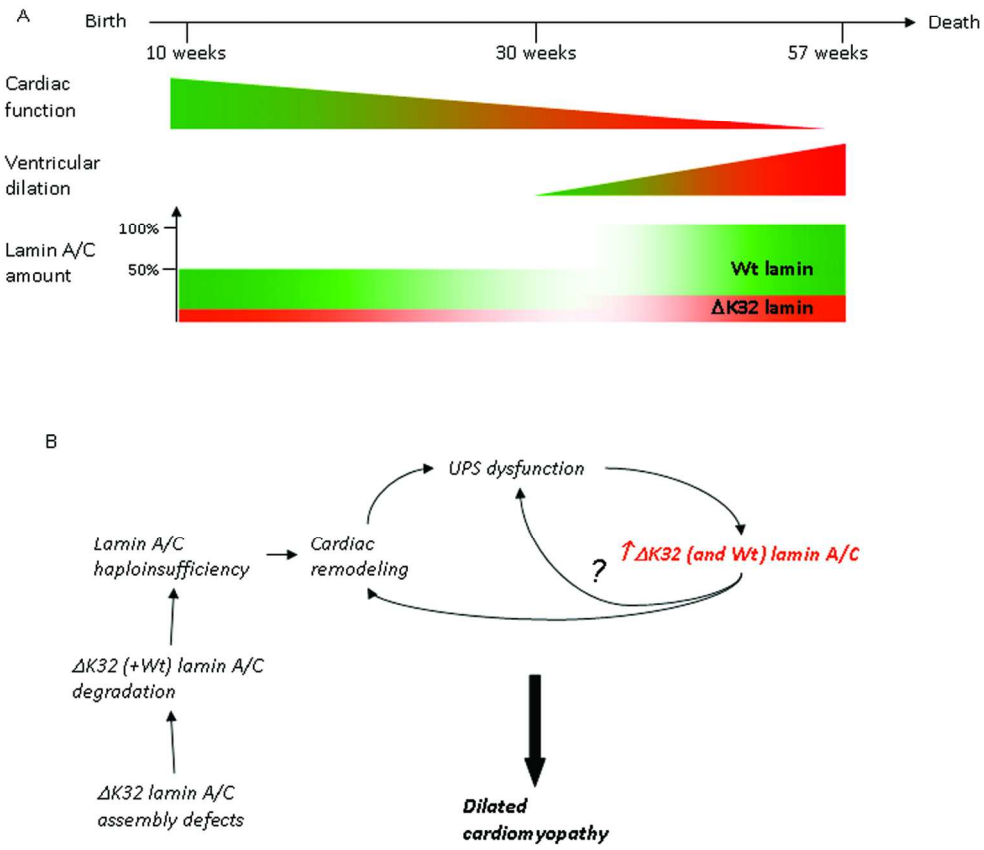

Figure 7. Schematic model of pathophysiological mechanisms linking ΔK32 lamin A/C to DCM. (A) Chronology of pathological events occurring in the heart of Het mice. (B) Working model suggesting that ΔK32 lamin A/C might disturb the assembly into protofilaments and thus be targeted for degradation (alone and/or associated to Wt lamin). It results in haploinsufficiency likely contributing to myocardial vulnerability, promoting remodelling mechanisms. These processes might have global deleterious effects, as UPS impairment. Wt and ΔK32-lamin A/C amount then increases, playing additional negative effects on cardiomyocytes function. This might precipitate cardiac dysfunction and UPS dysfunction (?), leading to DCM.

180x168mm (300 x 300 DPI)

Supplemental table 1. Skeletal muscle contractile properties in 57 week-old Wt and Het mice (number of animals). Iso N: specific maximal force during tetanic stimulation; TTP: time to peak measured during twitch stimulation; HRT: half-relaxation time measured during twitch stimulation. Mean ± SD.

		Wt	Het
Spontaneous activity test (13)			
Active time (% test duration)		79.2 ± 10.7	70.0 ± 22.4
EDL (7-8)	Muscle weight (mg)	12.1 ± 0.7	11.4 ± 1.5
	Iso N (N/mg)	135 ± 31	131 ± 41
	TTP (ms)	21.7 ± 3.0	23.1 ± 4.4
	HRT (ms)	21.9 ± 4.0	22.1 ± 4.0
Soleus (7-8)	Muscle weight (mg)	8.7 ± 1.7	7.8 ± 1.1
	Iso N (N/mg)	137± 41	129 ± 34
	TTP (ms)	46.7 ± 7.8	46.1 ± 13.1
	HRT (ms)	53.0 ± 17.0	74.1 ± 36.8
Diaphragm (7-8)	Muscle weight (mg)	6.3 ± 1.3	5.6 ± 1.6
	Iso N (N/mg)	97 ± 29	114 ± 33
	TTP (ms)	44.0 ± 8.0	44.0 ± 8.1
	HRT (ms)	42.9 ± 15.6	52.3 ± 14.3

Supplemental table 2. Echocardiographic parameters of Wt and Het male mice at 10, 30-40, 50-60 weeks of age. (number of animals). BW: body weight, IVSd: Interventricular septum thickness in diastole, PWd: Posterior wall thickness in diastole, LVED D: Left ventricular end-diastolic diameter, IVSs: Interventricular septum thickness in systole, PWs: Posterior wall thickness in systole, LVES D: Left ventricular end-systolic diameter, LVM: Left ventricular mass, FS: Fractional shortening, HR: Heart rate. **p<0.01 compared to age-matched Wt, Student t-test. Mean ± SD. Additional animals were added in the follow-up because death at some time points.

	10 weeks		30 - 40 weeks		50 - 60 weeks	
	Wt (13)	Het (14)	Wt (7)	Het (7)	Wt (7)	Het (7)
BW (g)	25.3 ± 3.2	23.9 ± 2.1	33.4 ± 4.5	30.5 ± 2.0 *	41.1 ± 5.4	29.5 ± 3.0 **
IVSd (mm)	0.67 ± 0.16	0.65 ± 0.13	0.44 ± 0.10	0.45 ± 0.06	0.44 ± 0.10	0.43 ± 0.08
PWd (mm)	0.83 ± 0.18	0.80 ± 0.17	0.49 ± 0.18	0.47 ± 0.12	0.49 ± 0.22	0.43 ± 0.09
LVEDD (mm)	3.61 ± 0.29	3.44 ± 0.29	3.63 ± 0.48	4.20 ± 0.43 **	3.55 ± 0.43	4.33 ± 0.49 **
IVSs (mm)	1.06 ± 0.22	1.10 ± 0.19	0.93 ± 0.17	0.78 ± 0.11 **	0.89 ± 0.07	0.70 ± 0.10 **
PWs (mm)	1.22 ± 0.14	1.19 ± 0.20	1.10 ± 0.20	0.91 ± 0.14 **	1.15 ± 0.20	0.84 ± 0.21 **
LVESD (mm)	2.10 ± 0.35	1.95 ± 0.30	2.24 ± 0.48	3.09 ± 0.64 **	2.18 ± 0.40	3.45 ± 0.72 **
LVM/BW (mg/g)	3.70 ± 1.02	3.41 ± 0.89	1.55 ± 0.71	2.13 ± 0.75 *	1.22 ± 0.63	2.31 ± 0.98 *
FS (%)	41.7 ± 7.0	43.5 ± 6.5	38.7 ± 6.8	26.9 ± 7.2 **	38.9 ± 5	20.9 ± 9 **
HR (bpm)	458 ± 56	479 ± 50	530 ± 38	525 ± 41	526 ± 40	559 ± 86

Supplemental table 3. Echocardiographic parameters of Wt and Het female mice at 10, 30-40, 50-60, 70-80 weeks of age. (number of animals). BW: body weight, IVSd: Interventricular septum thickness in diastole, PWd: Posterior wall thickness in diastole, LVED D: Left ventricular end-diastolic diameter, IVSs: Interventricular septum thickness in systole, PWs: Posterior wall thickness in systole, LVES D: Left ventricular end-systolic diameter, LVM: Left ventricular mass, FS: Fractional shortening, HR: Heart rate. *p<0.05 and **p<0.01 compared to age-matched Wt, Student t-test. Mean ± SD. Additional animals were added in the follow-up because death at some time points.

	10 weeks		30 - 40 weeks		50 - 60 weeks		70 - 80 weeks	
	Wt (7)	Het (8)	Wt (6)	Het (6)	Wt (7)	Het (7)	Wt (5)	Het (5)
BW (g)	20.2 ± 1.4	18.6 ± 1.4 *	25.5 ± 1.9	23.8 ± 2.2 *	28.8 ± 3.0	26.3 ± 2.1 **	31.1 ± 2.4	25.2 ± 4.5 **
IVSd (mm)	0.57 ± 0.13	0.60 ± 0.11	0.43 ± 0.09	0.42 ± 0.08	0.40 ± 0.04	0.38 ± 0.08	0.45 ± 0.11	0.44 ± 0.08
PWd (mm)	0.73 ± 0.16	0.78 ± 0.15	0.49 ± 0.20	0.48 ± 0.14	0.39 ± 0.07	0.38 ± 0.06	0.49 ± 0.19	0.47 ± 0.21
LVEDD (mm)	3.16 ± 0.27	3.18 ± 0.21	3.37 ± 0.41	3.33 ± 0.36	3.22 ± 0.33	3.54 ± 0.58	3.29 ± 0.28	4.19 ± 0.50 **
IVSs (mm)	0.99 ± 0.20	0.95 ± 0.18	0.88 ± 0.13	0.77 ± 0.11 **	0.83 ± 0.09	0.66 ± 0.13 **	0.93 ± 0.17	0.68 ± 0.21 *
PWs (mm)	1.07 ± 0.15	1.08 ± 0.22	0.97 ± 0.16	0.94 ± 0.12	1.02 ± 0.12	0.82 ± 0.14 **	1.06 ± 0.24	0.84 ± 0.28
LVESD (mm)	1.77 ± 0.39	1.86 ± 0.27	2.03 ± 0.40	2.11 ± 0.43	1.76 ± 0.34	2.49 ± 0.59 **	1.93 ± 0.24	3.35 ± 0.71 **
LVM/BW (mg/g)	2.97 ± 0.55	3.56 ± 0.86	1.69 ± 0.69	1.77 ± 0.67	1.18 ± 0.39	1.47 ± 0.60	1.14 ± 0.41	2.30 ± 1.36 *
FS (%)	44.4 ± 8.1	41.6 ± 6.7	39.9 ± 7.3	37.1 ± 8.2	45.6 ± 7.5	30.2 ± 7.9 **	41.3 ± 4.7	20.8 ± 9.6 **
HR (bpm)	450 ± 43	462 ± 64	505 ± 49	513 ± 62	541 ± 38	541 ± 47	542 ± 68	507 ± 75

Supplemental table 4. Oligonucleotides sequences for Q-PCR analysis.

cDNA target	Oligonucleotide	Sequence (5’ - 3’)
Nppa	For	AGCTTCCACCGAAGATAAC
	Rev	TCGTGATAGATGAAGGCAG
Nppb	For	GTCAGTCGTTTGGGCTGTAAC
	Rev	AGACCCAGGCAGAGTCAGAA
Myh7	For	GACCAGACCCCAGGCAAGGG
	Rev	GCCAACTTTCCTGTTGCCCC
Rplp0	For	CTCCAAGCAGATGCAGCAGA
	Rev	ATAGCCTTGCGCATCATGGT
Lmna	For	GCCAGCTCTACCCCACTGT
	Rev	CAGACTCAGTGATGCGAAGG
Lmna Wt	hydrolysis probe	TGCAGGAGAAGGAGGACCTGC
Lmna ΔK32	hydrolysis probe	CTGCAGGAGGAGGACCTGCAGG